Journal of Applied Physics

Trends in luminescence thermometry

Cite as: J. Appl. Phys. **128**, 040902 (2020); https://doi.org/10.1063/5.0014825
Submitted: 22 May 2020 • Accepted: 07 July 2020 • Published Online: 22 July 2020

Miroslav D. Dramićanin

Journal of Applied Physics PERSPECTIVE scitation.org/journal/jap

Trends in luminescence thermometry

Cite as: J. Appl. Phys. **128**, 040902 (2020); doi: 10.1063/5.0014825
Submitted: 22 May 2020 · Accepted: 7 July 2020 ·
Published Online: 22 July 2020

Miroslav D. Dramićanin[1,2,a)]

AFFILIATIONS

[1]College of Sciences, Chongqing University of Posts and Telecommunications, Chongqing 400065, People's Republic of China
[2]Vinča Institute of Nuclear Sciences—National Institute of the Republic of Serbia, University of Belgrade, PO Box 522, Belgrade 11001, Serbia

[a)]**Author to whom correspondence should be addressed:** dramican@vinca.rs

ABSTRACT

Following astonishing growth in the last decade, the field of luminescence thermometry has reached the stage of becoming a mature technology. To achieve that goal, further developments should resolve inherent problems and methodological faults to facilitate its widespread use. This perspective presents recent findings in luminescence thermometry, with the aim of providing a guide for the reader to the paths in which this field is currently directed. Besides the well-known temperature read-out techniques, which are outlined and compared in terms of performance, some recently introduced read-out methods have been discussed in more detail. These include intensity ratio measurements that exploit emissions from excited lanthanide levels with large energy differences, dual-excited and time-resolved single-band ratiometric methods, and phase-angle temperature readouts. The necessity for the extension of theoretical models and a careful re-examination of those currently in use are emphasized. Regarding materials, the focus of this perspective is on dual-activated probes for the luminescence intensity ratio (LIR) and transition-metal-ion-activated phosphors for both lifetime and LIR thermometry. Several particularly important applications of luminescence thermometry are presented. These include temperature measurement in catalysis, *in situ* temperature mapping for microfluidics, thermal history measurement, thermometry at extremely high temperatures, fast temperature transient measurement, low-pressure measurement via upconversion nanoparticle emission intensity ratios, evaluation of the photothermal chirality of noble metal clusters, and luminescence thermometry using mobile devices. Routes for the development of primary luminescence thermometry are discussed in view of the recent redefinition of the kelvin.

I. INTRODUCTION

Is luminescence thermometry a mature technology? This question is not easy to answer. The technique has long been known, having been introduced as early as the 1930s,[1,2] and many of its modern adaptations were envisaged by some of the earliest researchers in the field.[3,4] Nonetheless, the number of related publications and citations has increased almost exponentially with time,[5] and the number of published patents follows a similar trend. A recent Google search for patents using the terms "luminescence thermometry" and "phosphor thermometry" retrieved over 2800 results. Furthermore, these results typically are not incremental advancements. On the contrary, each year, we are witnessing new breakthrough advances in luminescence thermometry, in diverse scientific and technological fields. Moreover, in the last few years, two thematic books have appeared[6,7] and the first thematic conference was held in Scotland in 2018 (The Inaugural International Conference on Phosphor Thermometry—ICPT 2018). However, the widespread use of the method among non-experts and professionals has not been seen, even when its potential for the betterment of many measurements is obvious. These reasons explain why luminescence thermometry is not yet a mature discipline. In his fascinating paper on the history of luminescence thermometry, Allison[3] describes three eras in the development of the technique. At the present time, in my opinion, the field of luminescence thermometry is entering a fourth era, the era of maturity. To that end, further developments of the technique should be aimed at removing, or at least alleviating, inherent methodological problems and faults, to facilitate its widespread use.

Temperature measurement devices are abound. Again, a simple web search for commercial products using the term "temperature sensor" gives almost 1000 different possibilities, as stated by Talghader *et al.*[8] in their review article on thermal history sensors. Why, then, should we invest resources and effort into advancing luminescence thermometry? The answer to this question

is simple. Luminescence thermometry succeeds in environments where many other, if not all the existing, thermometry techniques fail. These environments include some that are of immense importance in nanotechnology, biomedicine, and optoelectronics. In biomedicine, for example, there is a strong need for precise temperature measurements at the intra- and inter-cellular levels. In addition, luminescence thermometry can be easily adapted to aid theranostics and nanotheranostics, since luminescence probes are inherently polyvalent materials. Besides thermometry, luminescence probes can be used for luminescence bioimaging, and many of them may also facilitate magnetic resonance imaging and x-ray computed tomography.[9] In addition, it has been demonstrated that up-converted light emitted by specially tailored nanoparticles can be used to trigger drug-release.[10–12] There are only a few thermometry methods with spatial resolutions of $<1\,\mu$m, with luminescence thermometry being one of them. Hence, the well-known historic Richard Feynman speech title on the emerging field of nanoscience, "There's plenty of room at the bottom," is appropriate as a description of the need for nanoscale thermometry methods. Today, we are able to routinely produce luminescent particles and structures of merely a few tens of atoms in size. These can be used not only to measure temperature but also to answer fundamental questions regarding the continuum and thermodynamic equilibrium at the nanoscale.

Being essentially a semi-contact method, luminescence thermometry can be used in environments that other methods cannot access. It can be exploited over a wide temperature range, having potential applications in cryogenic environments and in extremely high temperature settings, and it is usually possible to operate luminescence thermometry probes in harsh environments. Many engineering applications, such as flow temperature measurements or temperature measurements at engine surfaces, have benefited by using the method. Since the redefinition of the kelvin in 2018, primary thermometry has gained an additional significance at high (>1300 K) and low temperatures (around 1 K), because traceability may be directly linked to the redefined kelvin, instead of, as formerly, to a defined scale. Primary thermometry presents significant advantages over defined temperature scales in these temperature regions, whether owing to lower uncertainty or simply because of the ease of access to reliable thermometry.[13] Thus, the opportunity has arisen for the development and application of primary luminescence thermometry, especially at very high and low temperatures.

The scientific background of luminescence thermometry is well-established as it is mainly derived from existing extensive knowledge from the fields of luminescence and materials sciences. It is known that different applications require different approaches and probes in luminescence thermometry. However, the complex and interdisciplinary nature of many contemporary applications requires further acquisition of background scientific expertise and knowledge, which may be very demanding and far from trivial. In biomedicine, for example, the science behind *in vivo* measurements should include knowledge of real interactions between luminescence probes and biological constituents. In addition, in the same application field, there are serious concerns about the health and environmental impacts of materials used in luminescence temperature sensing and imaging, which have only been superficially considered so far. The long-term evolution of the properties of these probes also deserves further consideration. The widespread use of the method will only become a reality when these concerns have been properly addressed. Similar reasoning applies to all the various possible application fields, though each may face specific individual challenges.

This perspective follows the recent publication of reviews[5,14–35] and books[6,7] that comprehensively cover the techniques of temperature measurements via luminescence, materials used to prepare luminescence probes, and luminescence thermometry applications. For this reason, here, the aim is to outline recent trends in the development of the field, highlight innovative approaches in temperature read-out and probe materials, and point out novel and prospective applications. Note that the intention is not to provide a complete description of all the recent findings and developments but to discuss some recent results as indicators of the paths taken within the field of luminescence thermometry. Many parts of the text reflect the author's personal opinions and perspectives on the matters under discussion. The reporting of these opinions stems from the desire to help articulate current thinking, both about the goals to which this field should aspire in the forthcoming years—of which the overarching aim should be, in my opinion, to become a mature widespread technology—and regarding the strategy for achieving them.

II. TEMPERATURE READINGS FROM LUMINESCENCE

There are many ways to determine a temperature (temperature readouts) from luminescence, depending on the application. Likewise, many different materials can be used to construct a luminescence thermometry probe. The choice is mainly made according to the required working environment (e.g., bio-medical, nanoscale, or high-temperature engineering), operating temperature range, precision, thermometer complexity, and cost. But, in each case, the core of the luminescence thermometry application is a measurement. The objective of a measurement is to determine the value of the measurand, that is, the value of the particular quantity to be measured. In the case of thermometry, the measurand is the thermodynamic temperature, T. A measurement begins with an appropriate specification of the measurand, the method of measurement, and the measurement procedure.[36] Luminescence thermometry does not provide the value of the temperature directly; instead, it provides an indication (Q), which could be, for example, a ratio of emission intensities, luminescence lifetime, or a band shift. To be able to assess the quality of a measurement and to compare different types of measurements, one must determine the parameters which quantify measurement performance (figures of merit). The most important of these are the measurement range, absolute and relative sensitivities, temperature resolution, temporal resolution, spatial resolution, and the repeatability and reproducibility of the measurements. (The definitions of each of these parameters are given in Table I.) The difference between the smallest and the largest temperature that can be reliably measured by a thermometer determines its dynamic range (measurement range). The absolute sensitivity (S_a) of a thermometer is defined as a quotient of the change in an indication and the change in the temperature value, and it is expressed in terms of the indication unit per kelvin. The relative sensitivity (S_r) is defined as the ratio of the absolute sensitivity and the indication value. The temperature resolution (δT) is

TABLE I. Definitions of luminescence figures of merit, where Q is the indication (e.g., intensity ratio, lifetime, line-shift value), $\bar{Q}$ is the mean of individual observations Q_i, σ is the standard deviation of the measurements, and σ_r is the relative standard deviation of the measurements.

Thermometric parameter	Mathematical definition
Absolute sensitivity, S_a	$S_a = \left\|\frac{dQ}{dT}\right\|$
Relative sensitivity, S_r	$S_r = \left\|\frac{1}{Q} \times \frac{dQ}{dT}\right\| \times 100\%$
Temperature resolution, δT	$\delta T = \frac{\sigma}{S_a} = \frac{\sigma_r}{S_r}$
Spatial resolution, δx_{min}	$\delta x_{min} = \frac{\delta T}{\lvert dT/dx \rvert}$
Temporal resolution, δt_{min}	$\delta t_{min} = \frac{\delta T}{\lvert dT/dt \rvert}$
Repeatability, R	$R = 1 - \frac{\max\lvert \bar{Q} - Q_i \rvert}{\bar{Q}}$

the smallest change in a temperature that causes a perceptible change in the indication. The spatial resolution (δx_{min}) of a measuring system is defined as the minimum distance between the points of a measurement that can be resolved under the temperature resolution of the system, while the temporal resolution (δt_{min}) is the minimum period of time between measurements capable of resolving a temperature higher than the temperature resolution.

The repeatability is the measurement precision achieved during replicate measurements over a short period of time, under a repeatability measurement condition that comprises the same measurement procedure, measuring system, operator, operating conditions, and location; this, in fact, is the ability of the thermometer to provide the same result. Similarly, the reproducibility is the measurement precision under a reproducibility measurement condition that includes repeated measurements at distinct locations, using different measuring systems and operators. Both repeatability and reproducibility may be expressed quantitatively in terms of the dispersion characteristics of the results.[36]

Contrary to the situation in the earlier stages of luminescence thermometry development, recent papers generally report all figures of merit except for reproducibility. This considerably eases comparison between different luminescence thermometry methods and probe materials. However, the community should be aware of the importance of reproducibility in providing confidence in research results.[37] Even though such work may be challenging, in future, efforts must be made to undertake measurement comparison, establishment of consensus values, the optimization of reference material selection, and the determination of confidence limits, in order to advance the practice of luminescence thermometry.

To date, many different principles of temperature measurement from luminescence, so-called temperature readouts, have been demonstrated. Since practically all luminescence features are temperature-dependent to some extent, the inventive combination of these features may lead to new T-readouts, such as the recently reported dual-excited single-band and time-resolved single-band ratiometric readouts which will be discussed in more detail later in this section. Depending on the temporal nature of the observed luminescence phenomena, temperature readouts can be realized in steady-state, time-resolved, and frequency-domain measurement configurations. They differ in the complexity of the components needed for their realization (here, the term complexity also comprises the cost of instrumentation), their sensitivity to external disturbance, processing time, precision, and whether or not they require an external temperature reference element; read-out methods that do not require an external temperature reference are termed *self-referencing*. Table II presents a comparison of the typical characteristics of frequently used temperature readouts from luminescence.

Considering the number of papers published over the last two decades, spectral-shape-based thermometry realized by measurements of the luminescence intensity ratio (LIR) between two emission bands (ratiometric temperature readout) is the most popular choice for luminescence thermometry. This method is of paramount importance since it is self-referencing and hence problems caused by changes in measurement conditions are circumvented by relying on measurements of the ratios of absolute intensities. Compared to lifetime-based temperature readouts, which are also a very popular method, LIR T-readout is faster, simpler, requires less sophisticated instrumentation, and can be easily adapted for the thermal imaging. LIR can be monitored from luminescent probes containing one and two or more luminescence centers. LIR probes with a single emission center are usually lanthanide-ion-activated phosphors, and, in recent times, transition-metal-ion-activated phosphors, in which the ratio of emission intensities from two adjacent and thermally coupled excited states is utilized as a measure of temperature (Fig. 1).

The method is commonly termed Boltzmann-type LIR since thermally coupled excited states share are populated according to the Boltzmann distribution, and hence the ratio of emission intensities from these states can be presented with a simple equation,

$$\mathrm{LIR} = \frac{I_H}{I_L} = B \times \exp\left(\frac{-\Delta E}{kT}\right), \tag{1}$$

where I_H is the intensity of the emission from the higher-energy excited state, I_L is the intensity of the emission from the lower-energy excited state, ΔE is the energy difference between the thermalized excited states, and k is the Boltzmann constant ($k = 0.695\ \mathrm{cm^{-1}\ K^{-1}}$); in addition, $B = \nu_H A_H g_H / \nu_L A_L g_L$, where A is the radiative transition probability, ν is the emission barycenter frequency (or energy), and $g = 2J + 1$ is the level degeneracy. In this case, the relative sensitivity of LIR is a continuously decreasing function of temperature, and its value depends only on the energy difference between the thermalized excited states—the larger the difference, the larger the relative sensitivity,

$$S_R = \left|\frac{1}{\mathrm{LIR}} \times \frac{d\mathrm{LIR}}{dT}\right| \times 100\% = \frac{\Delta E}{kT^2} \times 100\%. \tag{2}$$

The largest energy gap between adjacent Ln^{3+} excited states is in the Eu^{3+} ion (between $^5D_1$ and $^5D_0$) and is approximately $1750\ \mathrm{cm^{-1}}$, meaning that the relative sensitivity varies with temperature as $251\,800/T^2$ (% $\mathrm{K^{-1}}$) and that the maximum achievable theoretical relative sensitivity of the technique is approximately 2.8% $\mathrm{K^{-1}}$ at 300 K for various hosts. Energy gaps of $\sim 1000\ \mathrm{cm^{-1}}$ in Dy^{3+} ($^4I_{15/2}$ and $^4F_{9/2}$), Sm^{3+} ($^4F_{3/2}$ and $^4G_{5/2}$), and Nd^{3+} ($^4F_{5/2}$ and $^4F_{3/2}$)

TABLE II. A comparison of different temperature readouts from luminescence.

Readout	Temporal character	Self-referencing	Instrumental setup complexity	Sensitivity to disturbance	Processing time	Precision
Emission intensity	Steady-state	No	Low	High	Short	Moderate
Band position	Steady-state	No	Low	None	Short	Very high
Bandwidth	Steady-state	No	Low	None	Short	High
Spectral shape (LIR)	Steady-state	Yes	Low	Low	Short	Moderate
Dual-excited single emission band	Steady-state	Yes	Low	Moderate	Moderate	Moderate
Emission decay time	Time-resolved	Yes	Moderate	Low	Moderate	Very high
Emission rise time	Time-resolved	Yes	Moderate	Low	High	Very high
Phase angle	Frequency-domain	Yes	Moderate	Low	Moderate	Very high
Time-resolved single emission	Time-resolved	No	High	Moderate	Moderate	Moderate
Polarization	Steady-state	Yes	High	Low	Short	High
Polarization lifetime	Time-resolved	Yes	High	Low	Moderate	High

provide relative sensitivities of 1.60% K^{-1} at 300 K, while smaller values of 1.25 and 0.93% K^{-1} at 300 K are achieved with Er^{3+} ($\Delta E = 780\ cm^{-1}$, between $^2H_{11/2}$ and $^4S_{3/2}$) and Pr^{3+} ($\Delta E = 580\ cm^{-1}$ between $^3P_1$ and $^3P_0$), respectively.[7,14] In the last couple of years, the ratio of emission intensities for the $^4T_2 \rightarrow {}^4A_2$ and $^2E \rightarrow {}^4A_2$ transitions of Mn^{4+} and Cr^{3+} have been examined with a view to their use in thermometry.[38–41] Their temperature sensitivities are similar to those of Ln^{3+}, but the deep-red and NIR emissions of these phosphors make them attractive for many applications and for especially biomedical uses.

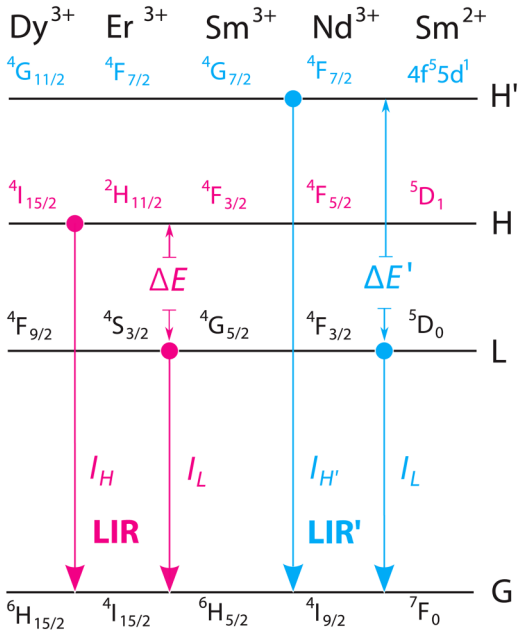

FIG. 1. Illustration of the emissions and energy levels involved in a luminescence intensity ratio (LIR) temperature readout. LIR is the conventional approach, utilizing emissions resulting from transitions from two adjacent excited levels (H and L), separated by the energy difference of ΔE, to the ground level (G). LIR′ indicates an approach in which an emission from a higher-energy excited level (H′) is used, where $\Delta E'$ denotes the energy difference between the emitting levels. LIR′ is more sensitive to temperature changes than LIR since $\Delta E' > \Delta E$. The terms of several trivalent lanthanide and divalent Sm ions with emissions that may be exploited for LIR and LIR′ are written near the lines representing the energy levels.

A. The intensity ratio of the emissions from a pair of excited levels with a large energy difference

Higher values of relative sensitivity for LIR can be achieved by utilizing a lanthanide emission from an excited state of higher energy than the first thermally coupled state, because of the larger energy difference, $\Delta E' > \Delta E$ (see Fig. 1). It is necessary, however, that a thermal equilibrium exists between these states. This approach is feasible, for example, in Dy^{3+}-activated phosphors, where a temperature-dependent intensity ratio between the 480-nm emission from $^4F_{9/2}$ excited state and the deep-blue 430-nm emission from the $^4G_{11/2}$ state, rather than the blue 458-nm emission from the $^4I_{15/2}$ state, may be used (the states are indicated in Fig. 1). The energy difference between $^4G_{11/2}$ and $^4F_{9/2}$ is approximately 2400 cm^{-1}, which provides a relative LIR sensitivity of 3.84% K^{-1}, a much higher value than in the conventional LIR utilizing emissions from the $^4I_{15/2}$ and $^4F_{9/2}$ states, as recently demonstrated by Li *et al.*[42] using Dy^{3+} activated $CaWO_4$ powders. In addition to the much exploited green and red emissions, an Er^{3+} ion also provides a weak blue emission from the $^4F_{5/2} \rightarrow {}^4I_{15/2}$ (≃450 nm), $^2P_{3/2} \rightarrow {}^4I_{11/2}$ (≃470 nm), and $^4F_{7/2} \rightarrow {}^4I_{15/2}$ (≃490 nm) transitions.[43] The intensity ratio between emissions originating from the $^4F_{7/2} \rightarrow {}^4I_{15/2}$ (≃490 nm) and $^4S_{3/2} \rightarrow {}^4I_{15/2}$ (≃550 nm) transitions is more sensitive to temperature changes than the conventional ratio of emissions originating from the $^2H_{11/2} \rightarrow {}^4I_{15/2}$ (≃530 nm) and $^4S_{3/2} \rightarrow {}^4I_{15/2}$ transitions,[44–46] (see Fig. 1), and can reach 3.6% K^{-1} at 300 K, as the energy difference between $^4F_{7/2}$ and $^4S_{3/2}$ is approximately 2260 cm^{-1}. Despite the greater sensitivity, the ratio between the emissions from $^4F_{7/2}$ and $^4S_{3/2}$ has been shown to provide about half the measurement resolution with respect to that given by the $^2H_{11/2}$ and $^4S_{3/2}$ ratio, 0.7 K vs 0.3 K.[46] An additional possibility is the LIR between Er^{3+} emissions from

the $^2G_{9/2}$ and $^2H_{9/2}$ states that are separated by $\Delta E \sim 2700\ cm^{-1}$; however, these emissions may be very weak. Energy differences between excited states larger than $2000\ cm^{-1}$, suitable for achieving a high relative measurement sensitivity, can be also found in Sm^{3+} ($^4G_{7/2}$ and $^4G_{5/2}$ states) and Nd^{3+} ($^4F_{7/2}$ and $^4F_{3/2}$ states), as shown in Fig. 1. Highly sensitive temperature readings using Nd^{3+} activated nanoparticles are favorable for biothermal imaging.[47,48] However, the higher relative sensitivity does not necessarily provide an overall benefit for temperature sensing from luminescence. Emissions from the high-energy excited states usually have lower intensities than those from the lower ones, so the uncertainty in measurements may be higher, which reduces temperature resolution, as was the case for the Dy^{3+} activated $CaWO_4$ powders.[42] Thermalization between f and d excited states in divalent lanthanide ion luminescence centers facilitates luminescence thermometry with a high relative sensitivity.[49] For example, the energy difference between $4f^55d^1$ and $^5D_0$ ($4f^6$) states in Sm^{2+}-doped SrB_4O_7 is relatively high (about $4000\ cm^{-1}$) (Fig. 1), which provides a relative sensitivity for LIR using the d- and f-emissions of about 6.4% K^{-1} at 300 K. Thermal coupling between these excited levels is possible due to strong electron–phonon coupling.

B. Dual-excited single-band ratiometric luminescence thermometry

LIR *T*-readouts have been recently extended to monitor the ratio of two intensities of emission, I_{EX1} and I_{EX2}, corresponding to the same upper state being excited by two different energies in succession.[50] This method is called *dual-excited single-band ratiometric thermometry* (LIR_{GE}), and it is schematically depicted in Fig. 2.

When the excitation energies correspond to Ln^{3+} ground and adjacent excited states, such as the Eu^{3+} ^7F_J levels, the temperature dependence of this LIR_{GE} follows the Boltzmann equation, just as in traditional LIR,

$$LIR_{GE} = \frac{I_{EX2}}{I_{EX1}} = B_{GE} \times \exp\left(\frac{-\Delta E_{GE}}{kT}\right), \tag{3}$$

because of the thermal equilibrium between excitation levels separated by the energy difference ΔE_{GE}. This approach has a few obvious advantages over the traditional two-emission LIR. The pre-exponential factor B_{GE} and ΔE_{GE} can both be straightforwardly obtained from the single measured emission spectrum. B_{GE} is the ratio of the integral of the emissions for the transition ending at the EX1 and EX2 states and ΔE_{GE} is determined as the energy difference between the barycenters of these emissions. Thus, there is no need to calibrate LIR_{GE} using an independent measurement of the temperature, in contrast to the conventional LIR, for which a new calibration procedure is required whenever the thermometer is operated in a different medium.[50] Furthermore, among all the possible luminescence thermometry read-out methods, LIR_{GE} requires the simplest sensor construction to monitor temperature.[51] Finally, the energy difference ΔE_{GE} can be large—for example, $\simeq 2230\ cm^{-1}$ between the Sm^{3+} states $^6H_{9/2}$ and $^6H_{5/2}$, $\simeq 1860\ cm^{-1}$ between Nd^{3+} $^4I_{11/2}$ and $^4I_{9/2}$, $\simeq 2060\ cm^{-1}$ between Tb^{3+} $^7F_5$ and $^7F_6$, and $\simeq 2160\ cm^{-1}$ between Pr^{3+} $^3H_5$ and $^3H_4$—and this results in a high-sensitivity *T*-readout. As illustrations of possible excitation combinations for this *T*-read-out method, energies of the ground level and adjacent excited levels for Eu^{3+}, Nd^{3+}, Sm^{3+}, Tb^{3+}, and Pr^{3+} in Y_2O_3 (in C_2 sites)[52,53] are given in Table III. Recently, Trejgis *et al.*[54] have demonstrated this type of luminescence thermometry, measuring a relative sensitivity of 2.95% K^{-1} at room temperature using Nd^{3+}-activated oxyfluorotellurite glass. The major drawbacks of this approach in luminescence thermometry are the necessity of measurement correction due to the bandwidth change with temperature as shown by Zhou *et al.*[55] and the need for constant switching between excitations. In addition, one should consider absorptions from trivalent ions located at multiple sites, for example, at S_6 sites in rare earth sesquioxides. These absorptions, even having very small intensities, may cause the deviation in the LIR from the theoretical value [Eq. (3)].

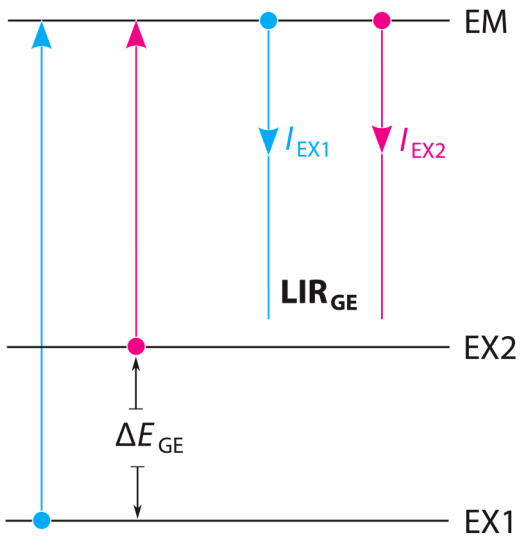

FIG. 2. Schematic representation of the principle of dual-excited single-band ratiometric luminescence thermometry, LIR_{GE}. The method is based on the ratio of the intensities of two emissions, I_{EX1} and I_{EX2}, from the same emitting level (EM) to two different lower energy levels, measured in response to successive excitations from EX1 and EX2. The required condition is that a thermal equilibrium exists between EX1 and EX2, which are separated by the energy difference of ΔE_{GE}. The intensity ratio of LIR_{GE} follows the same temperature dependence as that of the conventional LIR.

C. Time-resolved single-band ratiometric luminescence thermometry

LIR methodology can be further advanced if performed with time-resolved measurements. The ratio of emission intensities for the same emission band taken at the different time-delays after excitation ["time-resolved single-band ratiometric luminescence thermometry (TSBR)"] has been demonstrated by Qiu *et al.*[56] In this work, hybrid upconversion nanoclusters (UCL-NCs) comprised of PbS quantum dots (3.5 nm in size) and $NaYbF_4$:0.5%Tm@$NaYF_4$:10% Yb@$NaYF_4$:50%Nd (12 nm in size) were used to provide a short-lifetime emission centered at 814 nm and a long lifetime emission

TABLE III. Energies of the ground state and low-lying excited states of Eu^{3+}, Sm^{3+}, Nd^{3+}, Tb^{3+}, and Pr^{3+} in Y_2O_3 (C_2 sites).[52,53]

Eu^{3+}		Sm^{3+}		Nd^{3+}		Tb^{3+}		Pr^{3+}	
State $^{2S+1}L_J$	Energy (cm^{-1})	State $^{2S+1}L_J$	Energy (cm^{-1})	State $^{2S+1}L_J$	Energy (cm^{-1})	State $^{2S+1}L_J$	Energy (cm^{-1})	State $^{2S+1}L_J$	Energy (cm^{-1})
$^7F_0$	129	$^6H_{5/2}$	329	$^4I_{9/2}$	314	$^7F_6$	466	$^3H_4$	650
$^7F_1$	491	$^6H_{7/2}$	1336	$^4I_{11/2}$	2171	$^7F_5$	2524	$^3H_5$	2716
$^7F_2$	1185	$^6H_{9/2}$	2560	$^4I_{13/2}$	4133	$^7F_4$	3794	$^3H_6$	4851
$^7F_3$	2017	$^6H_{11/2}$	3867	$^4I_{15/2}$	6160	$^7F_3$	4749		
$^7F_4$	3005	$^6H_{13/2}$	5255						

centered at 804 nm, respectively. Upon 865-nm excitation, the ratio of the 810-nm emission intensity acquired after different time delays revealed a relative sensitivity of up to 5.6% K^{-1} and a thermal resolution of 0.5 K at 45 °C. Since both excitation and emission fall in the spectral region of the first biological window, the hybrid nanoprobe is suitable for use in biothermal imaging, as demonstrated by the authors using pork tissue slices of different thicknesses to simulate the rise in temperature of the nanoprobe in biological tissue. In the same study, the authors also performed *in vivo* thermal mapping of tumors in mice (Fig. 3). The breakthrough of this temperature readout is its insensitivity to tissue absorption and scattering. These two factors can considerably affect readouts based on the intensity ratio of emissions centered at different wavelengths since the magnitudes of both absorption and scattering vary with the light wavelength, and these variations can also vary between the same tissue type for different individuals (in-group variation).

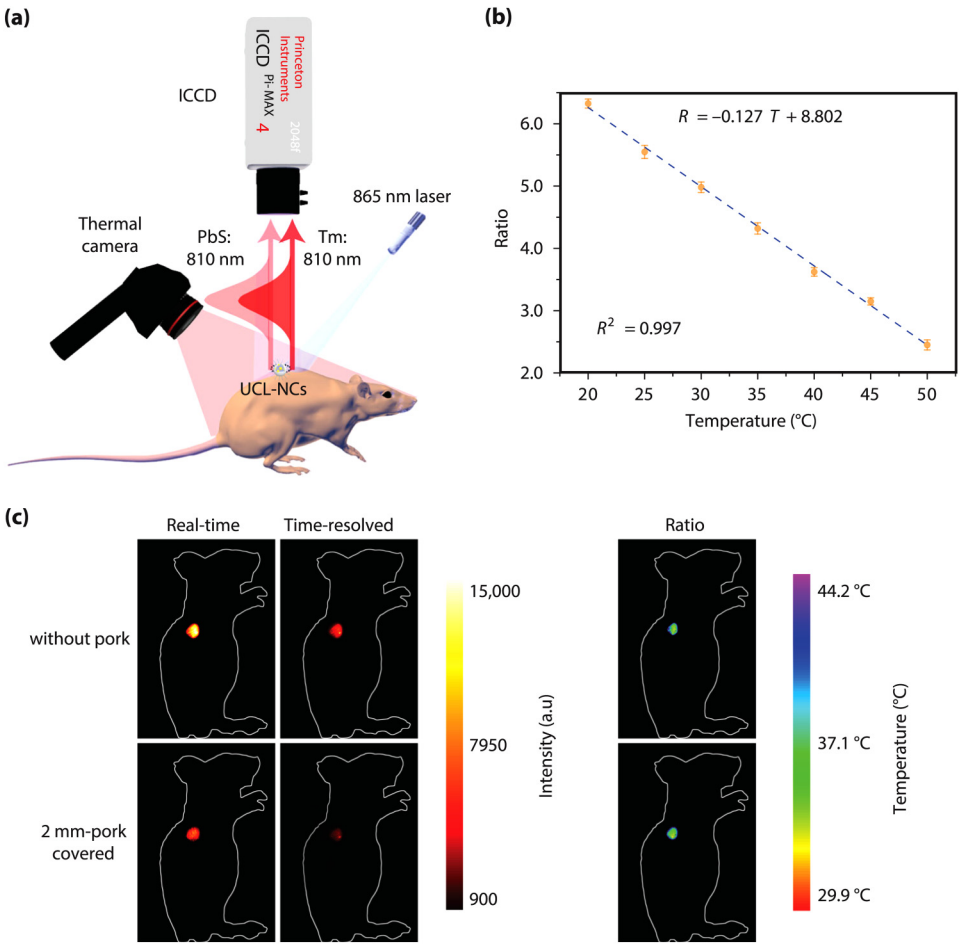

FIG. 3. *In vivo* temperature monitoring using upconversion luminescence hybrid nanoclusters (UCL-NCs) comprised of PbS quantum dots and $NaYbF_4$:0.5% Tm@$NaYF_4$:10%Yb@$NaYF_4$:50%Nd. (a) Schematic diagram of surface and intratumoral monitoring *in vivo*. (b) Standard curve for temperature evaluation *in vivo*, measured via a same-wavelength ratiometric probe based on UCL-NCs with 865-nm laser excitation, using a home-built time-gated bioimaging system. (c) Real-time, time-gated, and ratiometric UCL imaging *in vivo*, without and with a 2-mm pork-tissue slice covering the UCL-NCs, under irradiation by an 865-nm laser (0.5 W cm^{-2}) for 30 s. The ratio images (right) were obtained as the arithmetic image ratio [Ratio = (Real time−Time gated)/Time gated]. Reproduced with permission from Qiu *et al.*, Nat. Commun. **11**, 4 (2020). Copyright 2020 Author(s), licensed under a Creative Commons License (CC BY 4.0).

D. Highly sensitive dual-activated ratiometric intensity measurements

Regarding dual-activated luminescence temperature probes, in recent times, high-sensitivity LIR temperature readouts have been sought among different combinations of lanthanide (Ln) and transition metal (TM) ion emissions. These ions may be co-doped into a single host material or separated in different hosts comprising a binary mixture. Ln/TM-based LIR usually utilizes Ln ions for temperature-independent or slow-changing emission and TM ions for rapidly quenched emissions. Some recent examples include probes based on a Ho^{3+}:Y_2O_3 + Mn^{4+}:Mg_2TiO_4 binary mixture,[57] Dy^{3+},Mn^{4+}:$BaLaMgNbO_6$,[58] Er^{3+},Ni^{2+}:$SrTiO_3$,[59] Nd^{3+},Cr^{3+}:$Gd_5Al_{5-x}Ga_xO_{12}$,[60] Ce^{3+},Mn^{4+}:$Lu_3Al_5O_{12}$,[61] Eu^{3+},Mn^{4+}:$Y_3Al_5O_{12}$,[62] and Eu^{3+}:$GdVO_4$ + Cr^{3+}:Al_2O_3 hybrid particles.[63] The high sensitivity of these probes is a result of the strong *T*-quenching of the TM emission. Highly *T*-sensitive LIR probes can be constructed using this approach, taking advantage of the emissions of two lanthanide ions such as those in Nd^{3+},Eu^{3+}:YVO_4,[64] Ce^{3+},Tb^{3+}:YBO_3,[65] Ho^{3+}:Y_2O_3 + Er^{3+}:Y_2O_3, and Ho^{3+}:Y_2O_3 + Nd^{3+}:Y_2O_3 binary mixtures.[66] Kolesnikov *et al.*[64] obtained higher relative thermal sensitivity by using a Eu^{3+},Nd^{3+} co-doped YVO_4 probe and better thermal resolution by using the Eu^{3+}:YVO_4 + Nd^{3+}:YVO_4 binary mixture. The list of possible combinations of activator ions is long, and each combination can provide specific values for a thermometry measurement in terms of the spectral positions of the utilized emissions, achieved sensitivity, and resolution in different temperature ranges, etc. An example of such ingenuity in the optimization of dual-activated luminescence probes can be found in a paper by Pan *et al.*[67] They prepared Eu^{2+},Eu^{3+}:Sc_2O_3 nanoparticles via a thermal decomposition method using oleylamine as a solvent and a surfactant [Fig. 4(a)].

Oleylamine, however, also reduced the proportion of Eu^{3+} to Eu^{2+} ions, which had the effect of the nanoparticles exhibiting both characteristic Eu^{2+} d–f and Eu^{3+} f–f emissions, the former changing dramatically in intensity with temperature and the latter serving as a reference [Fig. 4(b)]. The strong temperature sensitivity of the Eu^{2+}/Eu^{3+} LIR (3.06% K^{-1} at 267 K) is easily distinguished by the naked eye from the temperature-induced color variations observed under 254-nm excitation [Fig. 4(c)].

The use of the host emission as the reference in LIR is another option when developing highly sensitive LIR probes. This can be accomplished by doping a TM metal into a semiconductor quantum dot (QD) and using the LIR of the TM and QD emissions. Examples of this type of probe include Mn^{2+}-doped ZnS QDs, presented in the paper by Wang *et al.*,[68] and Mn^{2+}-doped perovskite $CsPbCl_3$ QDs.[69] Similarly, the use of defect host emissions as the reference is also possible, and Eu^{3+}- and Sm^{3+}-doped anatase TiO_2 nanoparticles,[70,71] Dy^{3+}-activated $Gd_2Ti_2O_7$,[72] Eu^{3+}-activated $SrZrO_3$,[73] and Mn^{2+}-activated Zn_2SiO_4[74] have all been demonstrated as such. However, one should keep in mind that the reproducible preparation of probes having identical defect emission intensities is a difficult task.

E. Temperature readouts from the positions and bandwidths of emission bands

The usability of the temperature dependences of emission and excitation band positions and bandwidths for luminescence thermometry has long been a subject of debate. It had been thought that temperature-induced band shifts and bandwidth broadenings are too small to provide precise temperature measurements. However, such assumptions were based on early findings in lanthanide-activated phosphors, including the very small *T*-induced

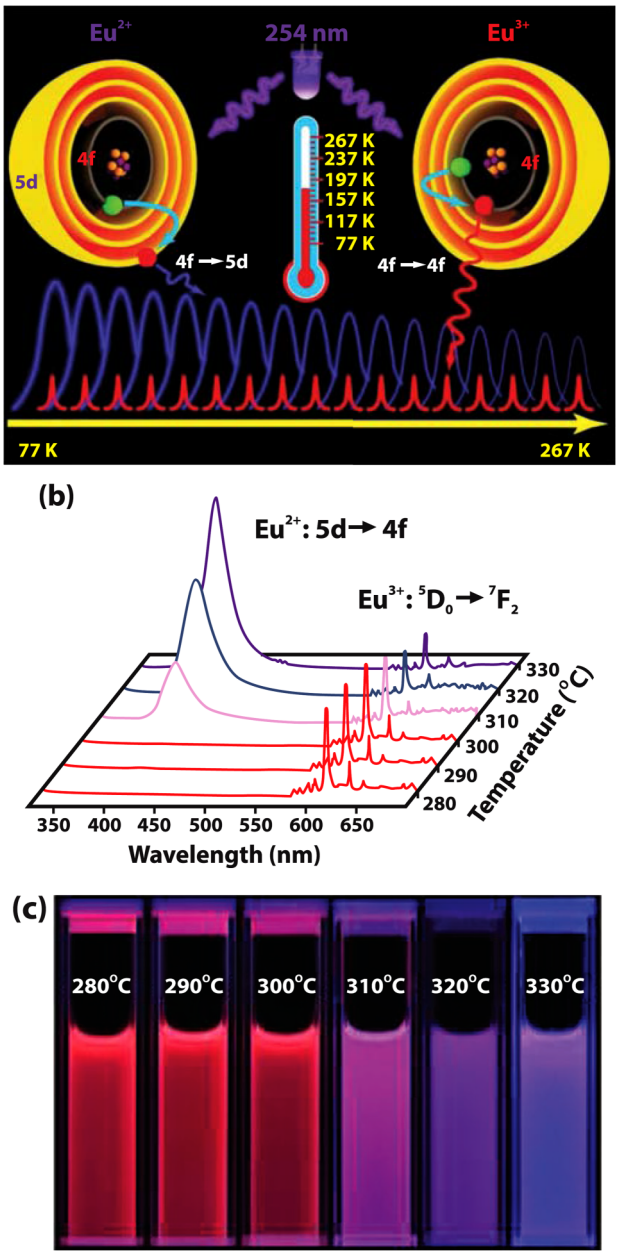

FIG. 4. Eu^{2+},Eu^{3+}:Sc_2O_3 luminescence thermometry nanoprobes. (a) Schematic of the operational principle. (b) Eu^{2+} d–f emission intensity strongly changes with temperature, while Eu^{3+} f–f emission intensity shows a slow change. (c) Temperature-induced variation of nanoparticle color observed under 254-nm excitation. Reproduced with permission from Pan *et al.*, Adv. Mater. **30**, 1705256 (2018). Copyright 2018 John Wiley & Sons.

shift of the Eu^{3+} $^5D_0 \rightarrow {}^7F_0$ emission band in Y_2O_2S[75] and the Nd^{3+} $^4F_{3/2} \rightarrow {}^4I_{9/2}$ emission band in LaF_3,[76] as well as an only 50-cm^{-1} bandwidth increase over a 630-K range for the Eu^{3+}:Y_2O_3 $^5D_0 \rightarrow {}^7F_2$ emission band.[77] Somewhat larger T-induced band shifts and broadenings have been observed for semiconductor quantum dots, for example, in CdTe QDs[78] and CdSe QDs coated with ZnS,[79] respectively, and in ZnO:Zn and ZnO:Ga.[80] However, recent studies[81–84] have shown that Ln- and TM-activated phosphors may present band shifts and band broadenings with adequate T-sensitivities, and hence their applicability for temperature sensing ought to be reconsidered, especially in light of the fact that the uncertainties in spectral measurements are quite low compared to, for example, uncertainties in intensity measurements. Ćirić *et al.*[81] have measured and analyzed T-dependent band shifts and band broadenings in Eu^{3+}- and Dy^{3+}-activated YVO_4. They found high relative sensitivities (>1% K^{-1} in the physiological range of temperatures—300–350 K) for the Eu^{3+} $^5D_0 \rightarrow {}^7F_1$ and Dy^{3+} $^4F_{9/2} \rightarrow {}^6H_{15/2}$ band positions. Kolesnikov *et al.*[82] have shown that the Nd^{3+}(2.4 at. %):YVO_4 $^4F_{3/2} \rightarrow {}^4I_{9/2}$ band shift has a temperature sensitivity of 0.75% K^{-1}, while Marciniak *et al.*[83] found relative sensitivities of 0.32 and 0.46% K^{-1} for the band shifts in Nd^{3+}-activated $LiLaP_4O_{12}$ and $LiNdP_4O_{12}$, respectively. Finally, in a very recent paper, Amarasinghe and Rabuffetti[84] showed a blueshift of 2.5% K^{-1} for the red emission band maximum ($^4T_2 \rightarrow {}^4A_2$) in Mn^{4+}:$Na_4Mg(WO_4)_3$ at 300 K.

F. Luminescence thermometry in the time and frequency domains

Time-integrated measurements, such as LIR and emission and excitation band shifts and broadenings, do not comprise all the information imparted by luminescence since they are merely an average of time-resolved phenomena. The decay or rise of emission intensity vs time, in the time-domain, and phase angles between harmonic excitation and emission, in the frequency domain, also show strong temperature dependences, and, thus, these can be used to determine temperature. Temperature readouts from excited-state lifetimes are very popular, owing to the fact that such measurements are self-referencing; lifetime values are not affected by the concentration and distribution of a probe material, nor are they influenced by fluctuations in excitation power, requiring the measurement of only one emission band. However, this method imposes strong limitations on the operational range of the thermometer, depending on the type of luminescence probe. For example, lanthanide-activated phosphors show negligible or very small lifetime changes at low and room temperatures, so they are suitable only for high-temperature applications.[14] The lifetimes of QDs also show small T-induced changes, the extent of change being notably dependent on QD size.[85] The rise times of emission show significant fluctuations around room temperature,[86,87] but these may not be detectable for many probes. The temporal dependence of the emission after pulsed excitation in such cases can be represented as[88–90]

$$I(t) = A \times [\exp(-t/\tau_d) - \exp(-t/\tau_r)], \tag{4}$$

where A is a constant, τ_d is the emission decay time, and τ_r is the emission rise time.

In the frequency domain, when the excitation is harmonically modulated, the phase angle (ϕ) between emission and excitation exhibits temperature dependences for both the decay and rise times. For Ln^{3+} upconversion phosphors, Liu *et al.*[90] derived an equation which relates the phase angle with τ_d and τ_r using a simplified rate equation model,

$$\phi = \arccos \frac{1 - \omega^2 \tau_d \tau_r}{\sqrt{(1 - \omega^2 \tau_d \tau_r)^2 + \omega^2 (\tau_d + \tau_r)^2}}, \tag{5}$$

where $\omega = 2\pi f$ is an angular frequency (f is the frequency). When the rise time is neglected ($\tau_r = 0$), Eq. (5) is reduced to the well-known equation[91]

$$\phi(\tau_r = 0) = \arccos \frac{1}{\sqrt{1 + \omega^2 \tau_d^2}}. \tag{6}$$

The excited-state lifetimes of TM-ion-activated phosphors show temperature dependences similar to those of Ln^{3+}-activated phosphors, but the temperature region in which the lifetime strongly changes with the temperature is different, usually corresponding to low and room temperatures. Phosphors activated with Cr^{3+} and Mn^{4+} (both having a $3d^3$ electron configuration) are of particular importance for luminescence thermometry since they efficiently emit in the red or deep-red spectral region, producing broad excitation bands in the visible spectrum. The temperature can be determined from their emission in three ways: from the ratio of emission intensities of the $^4T_2 \rightarrow {}^4A_2$ and $^2E \rightarrow {}^4A_2$ transitions, from the T-induced shift and broadening of the emission peak, and from the T-dependence of their relatively long excited-state lifetimes. Regarding the T-dependence of the lifetimes, Senden *et al.*[92] have shown that the temperature quenching of Mn^{4+} emission occurs by a thermally activated crossover, through the $^4T_2$ level, or by thermally activated auto-ionization (in the case of hosts with small energy bandgaps), both processes being described by the same expression[92–94]

$$\tau(T) = \frac{\tau_R(0) \tanh(h\nu/2kT)}{1 + [\tau_R(0) \tanh(h\nu/2kT)/\tau_{NR}] \exp(-\Delta E/kT)}, \tag{7}$$

where $\tau_R(0)$ is the radiative lifetime at $T = 0$ K, $h\nu$ is the average energy of the phonons coupled to the $^2E \rightarrow {}^4A_2$ transition, $1/\tau_{NR}$ is the non-radiative decay rate at high temperatures, and ΔE is the activation energy of the process. The absolute and relative sensitivities are[94]

$$S_a(T)\ [\mathrm{s\ K^{-1}}] = \frac{d\tau(T)}{dT} = -\frac{\tau_R(0) \exp\left(\frac{\Delta E}{kT}\right)}{2kT^2} \times \frac{h\nu \exp\left(\frac{\Delta E}{kT}\right) \mathrm{csch}^2\left(\frac{h\nu}{2kT}\right) + \frac{2\Delta E \tau_R(0)}{\tau_{NR}}}{\left(\exp\left(\frac{\Delta E}{kT}\right) \coth\left(\frac{h\nu}{2kT}\right) + \frac{\tau_R(0)}{\tau_{NR}}\right)^2}, \tag{8}$$

$$S_R(\mathrm{T})[\%\ \mathrm{K}^{-1}] = \left|\frac{1}{\tau(T)} \times \frac{\mathrm{d}\tau(T)}{\mathrm{d}T}\right| \times 100\% = \frac{h\nu \exp\left(\frac{\Delta E}{kT}\right) \mathrm{csch}^2\left(\frac{h\nu}{2kT}\right) + \frac{2\Delta E \tau_R(0)}{\tau_{NR}}}{2kT^2\left(\exp\left(\frac{\Delta E}{kT}\right)\coth\left(\frac{h\nu}{2kT}\right) + \frac{\tau_R(0)}{\tau_{NR}}\right)} \times 100\% . \quad (9)$$

The analysis presented in Ref. 94 shows that the excited-state lifetimes of Mn^{4+}-activated phosphors (the same analysis may be applied to Cr^{3+}-activated phosphors in which Cr^{3+} is in the so-called strong crystal-field environment) can be used for sensitive thermometry in different temperature ranges, depending on the properties of the host material (Fig. 5). Hosts having low phonon-coupling energies to the $^2E \rightarrow {}^4A_2$ transition and low values of the cross-over energy are favorable for use at low temperatures, while hosts with large phonon-coupling and cross-over energies can be exploited at high-temperatures. The high non-radiative rate results, unfavorable for traditional phosphor applications (LEDs), facilitate luminescence thermometry with a high relative sensitivity. The choice between Mn^{4+} and Cr^{3+} phosphors may be arbitrary. Generally, excited-state lifetimes of Mn^{4+} phosphors are shorter than those of Cr^{3+} phosphor, which means that the former are favored in applications that require high temporal resolution (for example, in luminescence thermometry of fluid flows). However, Cr^{3+} phosphors emit at longer wavelengths, well inside the first biological window, which suits biomedical and chemical sensing applications.

III. THEORETICAL MODELING

Progress in luminescence thermometry must be associated with the development of theoretical models and a careful re-examination of those currently in use. For example, the Boltzmann-type LIR method is frequently used and interpreted with the use of Eq. (1) without prior checks as to whether a Boltzmann equilibrium exists between the excited levels responsible for the LIR emissions. Meijerink and his collaborators[95,96] analyzed the conditions required for the existence of the Boltzmann equilibrium between two excited levels and found that these conditions were not met in the experiments presented in many reports. The absence of the Boltzmann equilibrium leads to a deviation of the T-dependence of the experimental data from that described by Eq. (1). As stated in Ref. 95, the Boltzmann equilibrium exists only when the equilibration of two

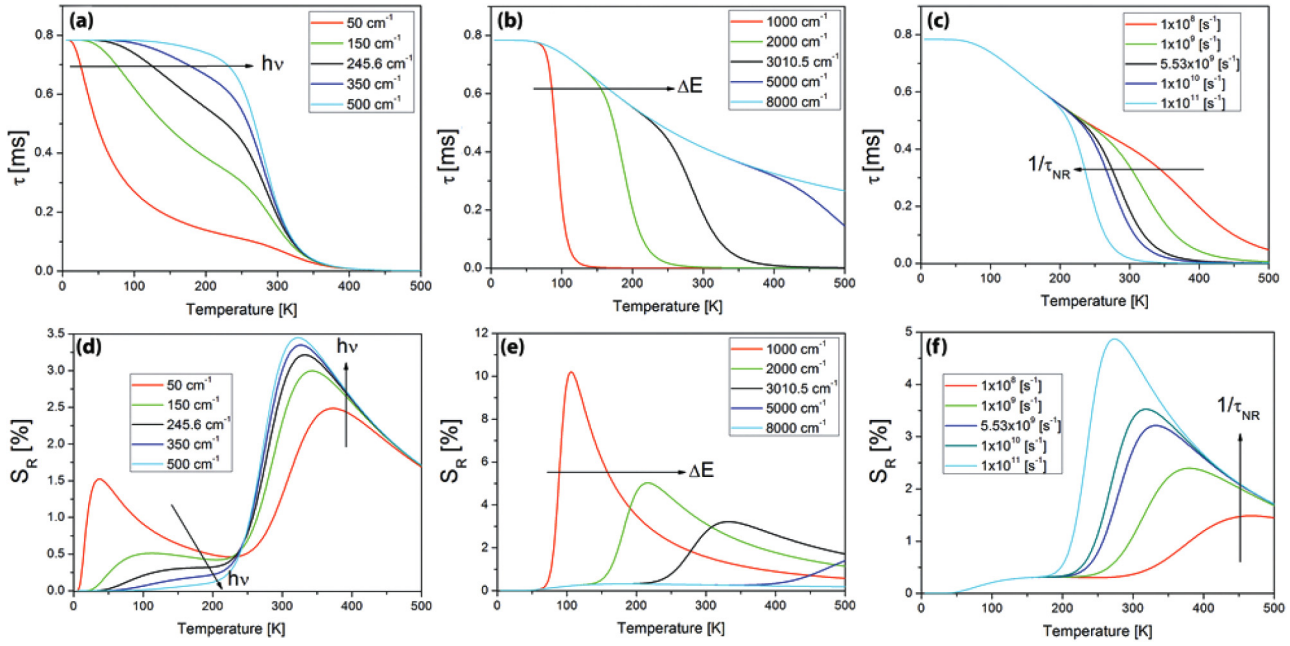

FIG. 5. Temperature dependence of emission decay time and relative sensitivity of Mn^{4+}-activated phosphor for (a) and (d) different values of phonon coupling energy $h\nu$, (b) and (e) different values of the crossover energy ΔE, and (c) and (f) different values of non-radiative decay rate $1/\tau_{NR}$. Note that lower values of the phonon coupling and crossover energies increase the relative sensitivity at lower temperatures and that the higher the non-radiative rate, the higher the relative sensitivity. Reproduced with permission from Dramićanin *et al.*, ChemistrySelect **4**, 7067 (2019). Copyright 2019 John Wiley & Sons.

thermally coupled states is fast in comparison with other processes affecting their population, notably, optical feeding and decay channels to the ground state. Thus, three different temperature behaviors of LIR of emissions from adjacent Ln excited states may occur, as illustrated in Fig. 6. The first, in which nonradiative relaxation is much faster than radiative decay, $1/\tau_{NR} \gg 1/\tau_R$, for which a Boltzmann equilibrium exists (left-hand side of Fig. 6). The second, in which nonradiative and radiative decay rates are similar, $1/\tau_{NR} \approx 1/\tau_R$ (middle section of Fig. 6), and the third, in which the radiative decay is faster than the nonradiative decay, $1/\tau_{NR} \ll 1/\tau_R$ (right-hand side of Fig. 6), do not follow Boltzmann statistics. For larger energy differences between excited levels ΔE, the relaxation between thermally coupled levels becomes slower, so deviations from Boltzmann equilibria occur more easily. Note that Ln activators with large ΔE values are frequently favored for LIR when high measurement sensitivity is needed. Therefore, it is of paramount importance to check for the existence of a Boltzmann equilibrium when exploiting LIR. The simplest way to do that is to perform time-resolved measurements and inspect emission decays from two excited levels. A single exponential decay, identical for emissions from both levels, is expected if a true Boltzmann equilibrium exists.[95] One way to overcome this problem and ensure a Boltzmann equilibrium is realized is to increase the concentration of Ln activators in the phosphor probe, which increases the non-radiative relaxation rate.

The use of theoretical modeling may reduce the requirements for experimental work, as demonstrated by Ćirić *et al.*[97] They showed that Judd–Ofelt intensity parameters derived from the room-temperature optical spectrum of a Ln^{3+}-activated phosphor can be used to calculate the thermometric properties of materials, as an LIR readout, with an error of less than 5%. Moreover, one can use the tabulated Judd–Ofelt intensity parameter values, which are abundantly available in the literature, to rapidly search for appropriate materials for sensor probes. Recently, this theoretical approach was extended to dual-excited single-band ratiometric thermometry.[51] Finally, it is important to mention that there are no reports on the use of materials informatics and data-driven approaches in luminescence thermometry research, to the best of author's knowledge. Given the immense developments in this field, it is reasonable to expect that such approaches may provide benefits in further luminescence thermometry developments.

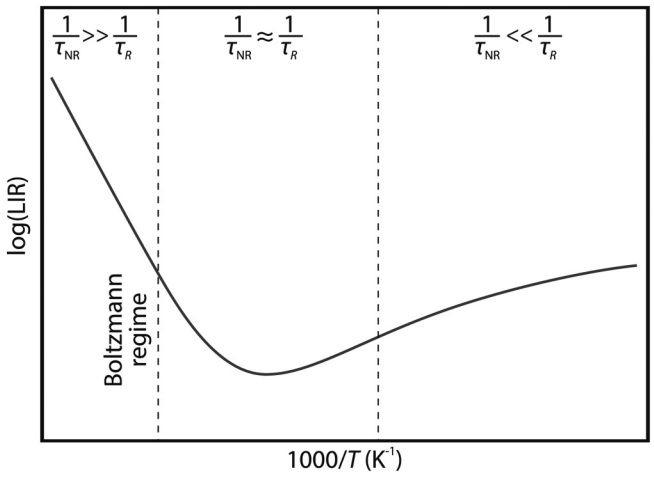

FIG. 6. Luminescence intensity ratio (LIR) plotted vs 1000/T showing three temperature regimes. In the case of $1/\tau_{NR} \ll 1/\tau_R$, LIR will decrease with temperature (right-hand side). In the case of $1/\tau_{NR} \approx 1/\tau_R$, there is a local minimum in the LIR (center). In the case of $1/\tau_{NR} \gg 1/\tau_R$, Boltzmann behavior determines an increase in LIR with T (left-hand side). Adapted from Geitenbeek *et al.*, Phys. Rev. Appl. **10**, 64006 (2018). Copyright 2018 Author(s), licensed under a Creative Commons License (CC BY 4.0).

IV. APPLICATIONS OF LUMINESCENCE THERMOMETRY

Today, luminescence thermometry has many applications in diverse research fields and environments, including electrical and mechanical engineering, biomedicine, nanotechnology, and microfluidics; for a comprehensive insight into luminescence thermometry applications, the reader may refer to two books[6,7] and the references therein. However, unsurprisingly, since temperature is one of the most commonly measured physical quantities and has effects on every aspect of our daily life, the field of applications of luminescence thermometry continues to expand. In this section, some of the novel and critical applications of luminescence thermometry are highlighted.

A. Catalysis

Recognized as one of the key chemical reactions for the advancement of civilization, catalysis has been extensively researched and, since the 1950s, has been a component of about 85%–90% industrial chemical processes.[98] Catalysis technologies have had, and continue to have, a strong positive impact on the preservation of the environment—for example, in atmospheric and wastewater depollution processing—and are backbones of the development of green chemistry for sustainable societies and the transition to carbon-neutral operations. The catalytic technology for methanol-to-olefins/aromatics/gasoline conversion is a promising alternative to classical production routes for high-demand chemicals and intermediates, helping to eliminate reliance on oil, to point-out just one among the many emerging uses of catalysis that are highly beneficial for the environment and promotion of sustainable development.[99] In catalysis research and applications, temperature is an essential parameter since it governs the reaction speed and influences the activation energy. Therefore, accurate temperature measurements of both the catalyst sample itself, as well as the reactants and products, are vital for comprehensive studies of catalytic reactions and processes.[100] Indeed, there is a particular requirement for temperature measurements to be performed under working conditions, which can be challenging. Previously, such measurements have been performed by using a variety of methods, such as IR thermography, multiple thermocouples, and NMR thermometry (see Ref. 101 and the references therein). For catalytic applications, however, these thermometry methods have serious drawbacks, such as low spatial resolution and complicated data analysis (as in the case of NMR thermometry). Recently, the great potential of luminescence thermometry for *in situ* temperature measurements during catalytic processes has been demonstrated in several papers.

Pfaff *et al.*[100] have demonstrated the use of luminescence thermometry for measurement of the temperature of a catalyst sample in a flow reactor, for heterogeneous catalysis, and showed that there was excellent agreement between this temperature and that determined by IR-thermometry. In this study, a $Mg_3F_2GeO_4:Mn^{4+}$ red-emitting phosphor was mixed with a magnesium aluminum silicate hydroxypropyl cellulose (HPC) binder and applied to the heating element in the reactor. The temperature was derived from the lifetime of the phosphor emission (excited by 266-nm Nd:YAG laser radiation), and a single shot accuracy of ±2 K was achieved. Geitenbeek *et al.*[101] mixed $NaYF_4:Yb^{3+},Er^{3+}$ microcrystalline upconversion particles with a commercial zeolite H-ZSM-5 to monitor the temperature at different heights in a reactor bed during a methanol-to-hydrocarbon catalytic reaction. By exploiting the ratio of the green upconversion emission intensities corresponding to the $^4I_{15/2} \rightarrow {}^4I_{15/2}$ and $^4S_{3/2} \rightarrow {}^4I_{15/2}$ transitions under 980-nm excitation, the authors were able to visualize a front of increasing temperature migrating down the fixed reactor bed, which occurs due to the exothermic nature of the catalytic reaction. A fiber probe, positioned in succession at different heights in the catalyst bed, was used to both excite and to collect the emission from the $NaYF_4:Yb^{3+},Er^{3+}$ particles. The uncertainty in measurement varied from 0.3 K, at the start of the catalytic reaction, to ca. 22 K, at later measurement times, due to the lowering of the emission signal intensity. Hartman *et al.*[102] used novel catalyst extrudate sensors that facilitate both luminescence thermometry and shell-isolated nanoparticle-enhanced Raman spectroscopy (SHINERS)[103,104] during the catalytic process of direct conversion of the synthesis gas (a fuel gas mixture consisting of hydrogen and carbon monoxide) into hydrocarbons. The catalyst extrudate sensors [Fig. 7(a)] consist of millimeter-sized SiO_2 extrudates supporting attached quasi-spherical $Au@SiO_2$ nanoparticles [Fig. 7(b), Au diameter ≈88 nm; SiO_2 shell thickness ≈2.6 nm], $NaYF_4:Yb^{3+}$, $Er^{3+}@SiO_2$ nanoparticles [Fig. 7(c), $NaYF_4:Yb^{3+},Er^{3+}$ core ≈25.4 nm, SiO_2 shell thickness ≈12.2 nm, Yb^{3+} concentration = 18 mol. % and Er^{3+} concentration = 2 mol. % Er^{3+}], and the Rh catalyst nanoparticles [Fig. 7(d)]. As for the previous example, the ratio of green upconversion emission intensities was used to monitor the temperature during an operando study of the catalytic reaction; a temperature measurement range extending to 900 K and a standard deviation of 0.3 K (calculated for >50 emission spectra) were achieved. Luminescence thermometry revealed the presence of a large offset of 50 K between the set reactor temperature and the catalyst temperature during CO hydrogenation, and a dependence on the CO/H_2 gas feed ratio at a constant flow speed resulting in temperature differences of up to 40 K.

B. Thermal history measurements and sensors

Thermal history sensors, also known as off-line thermometers, are used to provide forensic evidence of the temperatures that they experience during thermal events of interest. Such temperature

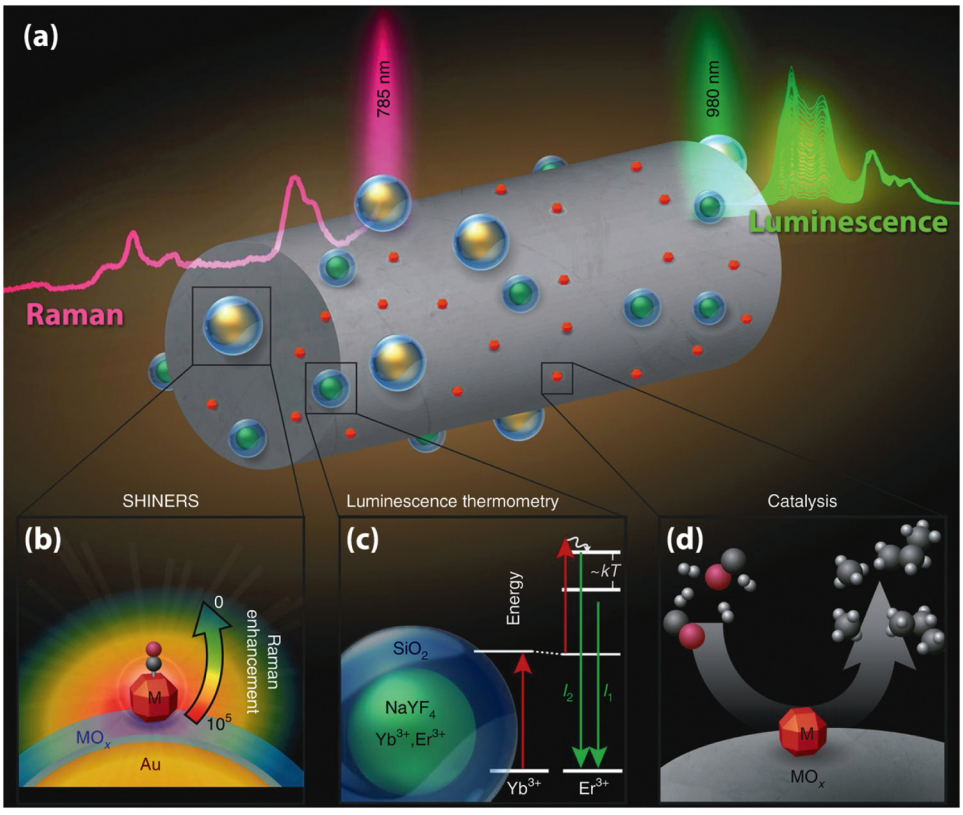

FIG. 7. Schematic illustration of a catalyst extrudate sensor for operando spectroscopy. (a) The gray SiO_2 extrudate carrying $Au@SiO_2$ shell-isolated nanoparticle (SHINs, gold quasi-spheres), $NaYF_4:Yb^{3+},Er^{3+}@SiO_2$ temperature sensors (green spheres), and Rh catalysts (red particles) to simultaneously measure temperature and surface species using luminescence thermometry and SHINERS. (b)–(d) Basic principles of SHINERS, $NaYF_4::Yb^{3+},Er^{3+}$ upconversion temperature sensors, and CO hydrogenation over a supported metal catalyst. Reproduced with permission from Hartman *et al.*, Nat. Catal. **2**, 986 (2019). Copyright 2019 Springer Nature.

recording is important for monitoring the integrity of pharmaceutical products, ensuring the quality of foods and beverages, and monitoring the degradation of consumer electronics, batteries, and even textiles.[105] It is also much needed in high-temperature environments for the development and safe use of chemical reactors, engines, and gas turbines. Furthermore, in some cases, off-line measurements are the only option to assess the temperature distribution at the location of interest during a thermal event, for example, in harsh environments, such as during laser annealing or an explosion.[8] The same is true for areas that are not physically accessible, such as the interior of high-temperature solid oxide fuel cells. In contrast to the abundance of traditional thermometers, thermal history sensors are rare and mostly still at the research stage, owing to the stringent requirements for their effective functioning. Such sensors should be based on an irreversible change of sensor properties with temperature and should be capable of following rapid temperature changes without damage, measuring and storing temperature and time in some manner without internal or external sources of power and free of communication, which requirements are not very compatible with the thermal event to be monitored. Temperature-sensitive paints and coatings (or thermal paints and coatings) are the best known and exploited thermal history sensors. These paints are made of metallic compounds (Pb, Co, Mg, etc.), binders, and solvents. Due to the chemical reactions of the metallic components at elevated temperatures, the paint permanently changes its color, and this color change indicates the highest temperature to which the paint was exposed. For thermal coatings, the inclusion of a binder is avoided to allow the thermal sensor to endure longer in harsh environments, but, as a result, its application requires complex deposition techniques. In general, the use of thermal paints and coatings requires cumbersome interpretation of data, the toxicity of the metal components in paints is problematic, color measurements may be compromised by metal fragments or other environmental components, and the method provides a temperature resolution that is at best 10 K.[106]

Thermographic phosphors in the form of powders, paints, and coatings, are an alternative to thermal history paints and coatings with exceptional potential, and may provide a solution for off-line temperature measurements in many, if not all, the above-mentioned fields. Contrary to "on-line" thermographic phosphors, whose emission properties must reversibly and reproducibly change with temperature, thermal history phosphors (TH-phosphors) should undergo irreversible changes in their emission properties with temperature change; the emission properties being any of those already mentioned that are exploited in luminescence thermometry (changes in emission shape, lifetime, etc.). So far, four processes that can promote thermally driven permanent changes in the luminescence of a phosphor during its exposure to elevated temperatures have been identified: (i) amorphous-to-crystalline transitions, i.e., the crystallization of the phosphor, (ii) phase-change processes, (iii) diffusion of ions into the host material, usually emission killer center ions, and (iv) the oxidation of dopant activator ions, for example, the oxidation of Eu^{2+} to Eu^{3+}. Compared to color measurements, luminescence measurements are unaffected by ambient conditions, the presence of metal fragments and environmental artifacts, and can provide considerably higher temperature and spatial resolutions. For off-line measurements, temporal resolution is not of particular importance.

Rabhiou[107] prepared amorphous Y_2SiO_5:Tb phosphor via a solgel technique. It was shown that upon heating, the crystallization of the phosphor resulted in a monotonic increase in the Tb^{3+} excited-state lifetime. A thermal history phosphor paint was prepared from the amorphous Y_2SiO_5:Tb phosphor and a commercial binder, applied to a 180-mm stainless-steel disk, and then exposed to heating for a period of 40 min using a propane torch [Fig. 8(a)]. During the heat exposure, the temperature of the upper surface of the disk was measured using thermocouples in contact with the surface; excellent agreement between the temperatures obtained from the emission decays and the thermocouples was demonstrated, as shown in Fig. 8(b).[107,108] Copin *et al.*[109] have shown that temperature-induced crystallization of solgel-prepared erbium-activated yttria-stabilized zirconia powder (YSZ:Er^{3+}) enables thermal history reading on account of large increases in the emission intensity and decay time over the 1223–1423 K and 1173–1373 K ranges, respectively. Estimated theoretical resolutions for these off-line measurements are between 0.3 and 1 K for the intensity and between 6 and 2 K for the decay time readouts—much higher than that achievable using thermal paints in the same temperature range. The different mechanisms causing irreversible changes in the phosphor emission, i.e., the thermally activated oxidation of activator ions, have been investigated by Rabhiou *et al.*[110] They showed that the oxidation of valence ions in the +2 state in $BaMgAl_{10}O_{17}$:Eu^{2+}, $BaMgAl_{10}O_{17}$:Eu^{2+},Mn^{2+}, and $SrAl_{14}O_{25}$:Eu^{2+} can be used for emission-intensity ratio based thermal history recording over the 600–1300 °C range. In addition, because annealing phosphor powders in an Ar atmosphere at 1400 °C reduces the activator ions to their initial valence state, these sensors may be reusable.[111]

C. Measurement and sensing of physical properties other than temperature

Over the years, luminescence thermometry has been successfully used to substitute or complement measurement techniques for the sensing and measurement of various important physical properties or processes other than temperature. For example, the use of luminescence thermometry for temperature measurements in gas and liquid flows has been demonstrated and is still being extensively researched, as recently reviewed by Abram *et al.*[35] Future developments, as suggested in that review, may be concerned with three-dimensional "tomographic" temperature and velocity measurements, and the identification and/or production of more suitable phosphor particles, having near-spherical shapes, narrow size distributions, and higher brightness, to improve measurement accuracy. Considering the immense importance of controlling and measuring temperatures in microfluidic devices,[7] exploration of the possibilities for luminescence thermometry in this application field continues. The ideal temperature measurement technique for a microfluidic device should possess the following characteristics: (i) high spatial and temperature resolutions, (ii) high acquisition rate (temporal resolution), (iii) non-invasiveness, (iv) inertness in a solvent, and (v) the thermometer material should be light- and heat-resistant.[112] Luminescence thermometry meets these criteria

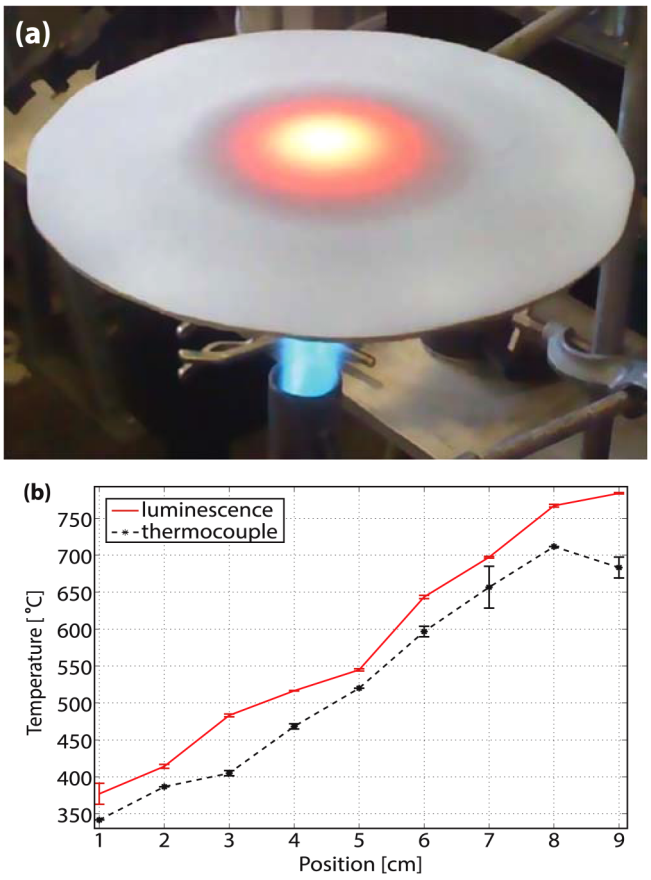

FIG. 8. Evaluation of thermal history using a Y_2SiO_5:Tb phosphor-based paint. (a) Stainless-steel disk painted with an amorphous Y_2SiO_5:Tb phosphor dispersed in a commercial binder heated from below for a period of 40 min by a propane torch. (b) Radial temperature distribution obtained using a thermocouple compared to the temperature determined from the excited-state lifetime of the phosphor at points adjacent to a thermocouple. Reproduced with permission from Heyes *et al.*, AIP Conf. Proc. **1552**, 891 (2013). Copyright 2013 AIP Publishing LLC.

since it can combine the high relative thermal sensitivity (>1% K^{-1}) and spatial resolution (<10 μm) in short acquisition times (<1 ms). So far, organic dyes have mainly been used for luminescence thermometry in microfluidic devices. However, dyes suffer from photobleaching, may react with fluids, and have limited measurement ranges due to degradation. These drawbacks may be overcome by adopting inorganic probes, as recently shown by Geitenbeek *et al.*,[113] who showed that the ratio of Er^{3+} emission intensities in $NaYF_4$ nanoparticles can be used for *in situ* temperature mapping with a temperature resolution of 0.34 K and a spatial resolution of ca. 1 mm. Further progress is expected in measurements of fast thermal transients by high-speed phosphor thermometry (HSPT). Such measurements are needed in internal combustion engines, swirl-stabilized gas turbine model combustors, turbulent flows, etc., where conventional thermometry methods, such as optical pyrometry, are infeasible.[114,115] The improved quality and reduced cost of high-speed photodetectors, such as high-frame-rate CMOS cameras,[116] as well as the increased availability of bright fast-decaying phosphors, should prove beneficial for future HSPT applications. In addition, new approaches for temperature determination are welcomed, and some, such as the use of the anti-Stokes luminescence of YAG:Ce^{3+},[115] are actively being investigated.

Research also continues on the development of luminescence thermometry for extremely high temperatures, which is important for modern turbine engines where the temperature limits for luminescence thermographic materials are tested.[117] Recently, Allison *et al.*[117] developed high-temperature luminescence-based fiber optic thermometry for temperatures up to 1700 °C. The optical system designed in this study was comprised of a Nd:YAG 355-nm laser injected into one leg of a flexible bifurcated optical fiber connected to a sapphire light pipe positioned in proximity to YAG:Dy^{3+} or YAG:Dy^{3+},Er^{3+} crystalline cylindrical probes (Fig. 9). The Dy^{3+} emission was measured after passing through another arm of the bifurcated fiber, a filter, and a lens, by a PMT detector. Temperature values were determined from the emission decay times, with sensitivities of 1% K^{-1} at 1400 °C and 0.9% K^{-1} at 1700 °C. At approximately the same time, Anderson *et al.*[118] demonstrated thermometry based on emission intensity ratios up to 1773K, using a YAG:Dy^{3+} thin film as a phosphor probe, and detecting Dy^{3+} luminescence to 2033K. Moreover, with this technique, high-speed temperature measurements (at rates up to 80 kHz) were shown to be possible under laboratory conditions.

Runowski *et al.*[119] converted a luminescent thermometer (YVO_4:Yb^{3+},Er^{3+}) into a remote vacuum sensor. First, they demonstrated enormous enhancement of light-to-heat conversion and heating of the YVO4:Yb^{3+},Er^{3+} particles under irradiation by a 975-nm laser in a vacuum, compared to the heating effects observed under ambient conditions, when air molecules transfer the generated heat to the surroundings and cool the particles [Fig. 10(a)]. Then, they showed that on account of pressure–temperature interdependence, pressures can be measured from the temperature-induced Er^{3+} emission intensity ratio change (525/550 nm) [Fig. 10(b)], in the pressure range from 0.07 to 10 mbar; sensitivities ranging from 500% $mbar^{-1}$ to 1% $mbar^{-1}$ and

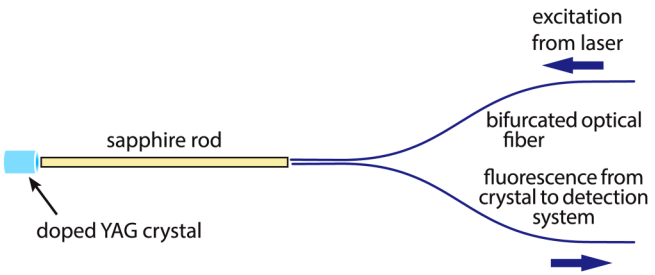

FIG. 9. Schematic of the fiber optic luminescence thermometry probe for emission decay time temperature measurements up to 1700 °C using YAG:Dy^{3+} or YAG:Dy^{3+},Er^{3+} crystal phosphors. Reproduced with permission from Allison *et al.*, Meas. Sci. Technol. **31**, 044001 (2020). Copyright 2019 IOP Publishing.

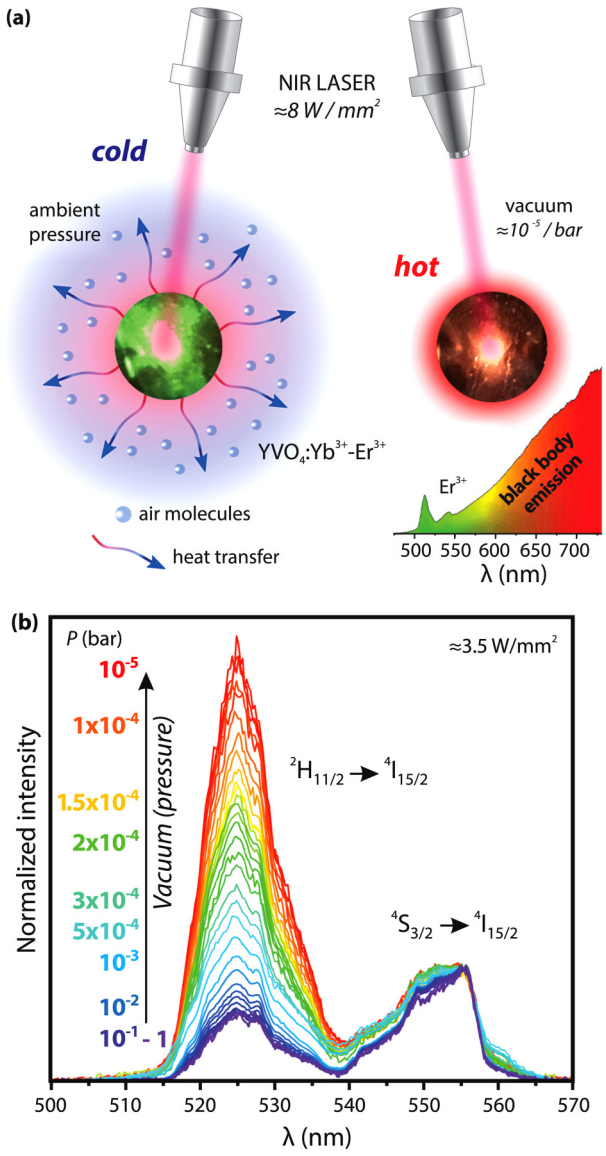

FIG. 10. Measurement of low pressures by luminescence thermometry. (a) Scheme of 975-nm laser-induced heating of YVO_4:Yb^{3+},Er^{3+}, at ambient pressure and in a vacuum; under ambient conditions, air molecules transfer the generated heat to the surroundings and cooldown the sample, whereas, in a vacuum, intense heating of the sample occurs. (b) Emission spectra of the YVO_4:Yb^{3+},Er^{3+} sample (975-nm laser excitation at an optical power density of 3.5 W/mm^2), normalized to the intensity of the $^4S_{3/2} \rightarrow {}^4I_{15/2}$ transition emission, recorded in the pressure range from $\approx 10^{-5}$ to 1 bar. Adapted with permission from Runowski *et al.*, Adv. Mater. Technol. **5**, 1901091 (2020). Copyright 2020 John Wiley & Sons.

resolutions from 0.1 to 10 mbar, depending on the nominal pressure were recorded. Besides being a highly innovative application, the importance of this result lies in the fact that it suggests that luminescence probe heating must be considered for luminescence thermometry testing and applications in low-pressure environments, for example, when performing measurements at low temperatures in vacuum cryostats. Another recent example of luminescence thermometry for measurements of physical properties other than temperature was reported by Miandashti *et al.*,[120] who used luminescence thermometry to study the photothermal chirality of Au helicoid nanoparticles. They spin-coated helicoid nanostructures on an AlGaN:Er^{3+} thin film and used a 532-nm laser for photothermal and photoluminescence excitation of gold nanostructures and Er^{3+}. In the course of this experiment, the optical and photothermal handedness, and an absolute temperature difference of 6 K between right- and left-circularly polarized light, were identified.

D. Luminescence thermometry using mobile devices

Recent sensor strategies have foreseen future designs of compact, lightweight, portable, and low-cost sensor systems.[121] Smartphones may become a platform for the construction of next-generation cost-effective hand-held sensors, due to their portability and ubiquitous availability (with an estimated more than two billion users worldwide). Such immense availability provides a large number of potential subscribers for smartphone-based sensor systems.[121] Smartphone-based measurements of optical spectra and emission lifetimes have been already demonstrated in several papers.[122,123] Pan *et al.*[122] demonstrated temperature measurements by observing changes in the TiO_2 thin film reflection spectrum using a smartphone. Zhu[123] presented a method to record upconversion emission decays with a low-cost and miniaturized apparatus consisting of a smartphone equipped with a 980-nm CW laser and motor.[123] As well as the basic display by smartphones of methods for luminescence measurements, several smartphone-based luminescence sensing applications for consumer goods monitoring have been published recently. Araque *et al.*[124] published a technique for the determination of gaseous oxygen concentrations inside packed foods based on the use of a luminescent membrane sensitive to O_2, optically excited and read by a smartphone. Ramalho *et al.*[125] introduced smart luminescence quick response (QR) codes, which can be used to store information as well as to sense the temperature in real time via the acquisition of a photograph using the charge-coupled device of a smartphone (Fig. 11). Organic–inorganic hybrids with europium (Eu^{3+}) and terbium (Tb^{3+}) ions used in the preparation of the QR codes provide information on the temperature to which the QR code is exposed, based on the intensity ratio of red and green pixels of an image obtained by the smartphone.

E. Toward primary luminescence thermometry

Two important events occurred in the last couple of years: the redefinition of the kelvin and the appearance of first papers describing attempts at primary thermometry realization using luminescence. The most radical revision of the International System of Units (SI) since its inception occurred in 2018. Now, all the SI units are based on the defined values of seven fundamental constants of nature.[13] The kelvin (K), the SI unit of thermodynamic temperature, is defined in terms of a fixed numerical value of the Boltzmann constant k of 1.380 649×10^{-23}, when expressed in units of J K^{-1}, which is equivalent to kg m^2 s^{-2} K^{-1}, where the kilogram, meter,

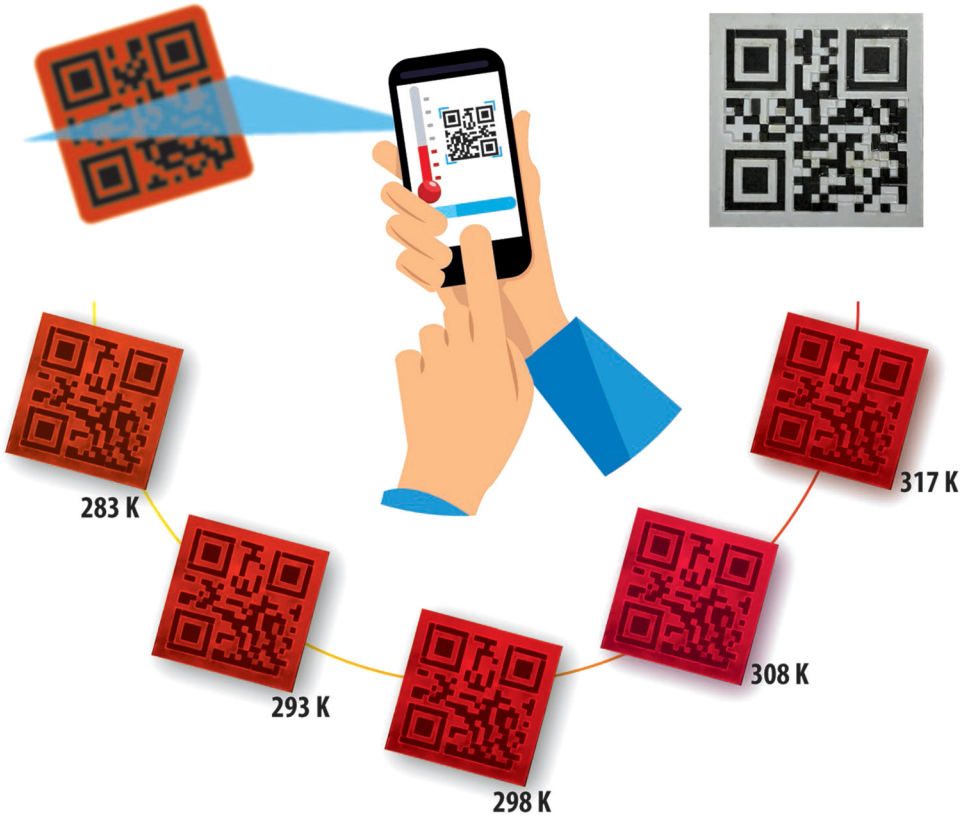

FIG. 11. Temperature sensing and message decoding using a smartphone to read the luminescent QR codes. The thermal dependence of the colors of the luminescent QR codes is also illustrated schematically. Adapted from Ramalho *et al.*, Adv. Sci. **6**, 1900950 (2019). Copyright 2019 Author(s), licensed under a Creative Commons License (CC BY 4.0).

and second are defined in terms of h, c, and $\Delta\nu_{Cs}$.[126] In this definition, h is the Planck constant ($h = 6.626\,070\,15 \times 10^{-34}$ J s or kg m^2 s^{-1}), c is the speed of light in a vacuum ($c = 299\ \ 792\ \ 458$ m s^{-1}), and $\Delta\nu_{Cs}$ is the unperturbed ground-state hyperfine transition frequency of the cesium-133 atom ($\Delta\nu_{Cs} = 9\ \ 192\,631\,770$ Hz). In effect, this definition means that one kelvin is equal to the change in thermodynamic temperature that results in a change of thermal energy kT by $1.380\,649 \times 10^{-23}$ J. Since this definition gives an exact relation between the Boltzmann constant and the SI units, $k = 1.380\,649 \times 10^{-23}$ kg m^2 s^{-2} K^{-1}, the inversion of this relation gives an exact expression for the kelvin in terms of the defining fundamental constants k, h, and $\Delta\nu_{Cs}$,[126]

$$1\,\mathrm{K} = \frac{1.380\ 649\ \times 10^{-23}}{(6.626\ 070\ 12\ \times 10^{-34})(9\ 192\ 631\ 770)}\frac{\Delta\nu_{Cs}h}{k} = 2.266\ 665\ 3\frac{\Delta\nu_{Cs}h}{k}. \tag{10}$$

The redefinition of the kelvin in terms of the Boltzmann constant has no effect on the temperature values or realization uncertainties of the two currently defined temperature scales (ITS-90 and PLTS-2000).[127] However, with the new definition, primary realizations of the kelvin can be established at any point of the temperature scale, which is significant for thermometry at low (<20 K) and high (>1300 K) temperatures and opens space for the development of primary luminescence thermometry for different environments.

When considering materials and methods for luminescence-based temperature readouts for the realization of primary thermometry, one must strictly adhere to the criteria stated as follows: "For primary-thermometry methods, a well derived equation of state describing the relation between thermodynamic temperature and other independent quantities of the physical system used must exist that does not contain unknown or significantly temperature dependent parameters."[128] Certainly, equations of state exist for each luminescence temperature readout. For example, the variation of the luminescence lifetime τ can be represented by the Mott–Seitz model,

$$\tau(T) = \frac{\tau_0}{1 + C \times \exp(-\Delta E/kT)}, \tag{11}$$

where $C = \tau_0/\tau_{NR0}$ and it is assumed that the probability of radiative processes is independent of temperature ($A_R = \text{const.} = 1/\tau_0$), while the probability of nonradiative process has a temperature dependence described by a Boltzmann factor of the form $A_{NR}(0) \times \exp(-\Delta E/kT)$; $A_{NR}(0) = 1/\tau_{NR0}$ is the non-radiative transition rate when $T \to 0$ and ΔE is the activation energy of the nonradiative process. Typically, the radiative lifetime τ_0 can be easily obtained by extrapolating the measured lifetime to absolute zero temperature, $\tau(T \to 0) \cong \tau_0$. Then, if $1/\tau_{NR0}$ and ΔE are

derived independently from thermometry measurements, and if they do not show temperature dependence, lifetime-based luminescence primary thermometry may be achieved, based on the following equation of state:

$$T(\tau) = \frac{\Delta E}{k \times \log\left(\frac{C\tau}{\tau_0 - \tau}\right)}. \quad (12)$$

A similar approach for obtaining the equation of state can be performed with other models that describe temperature variations of luminescence lifetimes, such as those that include multiphonon relaxation or quenching via charge-transfer band,[14] but with more complex equations and a larger number of parameters that must be independently derived.

The full width at half maximum (FWHM) of the emission peak of a lanthanide activated phosphor as a function of temperature ($\delta E(T)$) can be described by[129]

$$\delta E(T) = \sqrt{8\log 2}(h\nu)\sqrt{S\coth(h\nu/2kT)}, \quad (13)$$

using the Huang–Rhys factor (S) and the mean phonon energy ($h\nu$) of the host, which can be calculated independently.[130] The inverse of this function gives the equation of state for the determination of temperature from the emission peak bandwidth (valid only for $\delta E > h\nu\sqrt{8\log 2\, S}$),

$$T(\delta E) = \frac{h\nu/k}{\log\left(\frac{\delta E^2 + 8\log 2(h\nu)^2 S}{\delta E^2 - 8\log 2(h\nu)^2 S}\right)}. \quad (14)$$

In semiconductors, emission peak energy variations with temperature are frequently described by the empirical Varshni relation[131]

$$E_g(T) = E_{g0} - \frac{\alpha T}{\beta - T}, \quad (15)$$

where E_{g0} is the value of the semiconductor energy bandgap at 0 K, and α and β are the material constants. Clearly, the equation of state can be easily derived from the Varshni relation as a solution of a quadratic equation.

Regarding the luminescence intensity ratio (LIR) Boltzmann-type temperature readout, the realization of the primary thermometer may present a considerable challenge, even though the equation relating LIR and T is very simple [Eq. (1)]. The challenge arises due to the fact that parameters in Eq. (1) (B and ΔE) cannot really be considered to be temperature independent over a relatively wide temperature range. B incorporates the radiative transition probabilities and emission barycenter energies of two transitions, which vary with temperature, although weakly. The same stands for the energy difference between the excited levels, ΔE. This problem may be overcome by introducing an approximation for the temperature dependences. Finally, one should consider that if the equation of state is based on an approximation of a complex theory, it must at least be possible to estimate the order of magnitude of the deviation from theory.[128]

Recently, several attempts at the realization of primary luminescence thermometry have been made, and three examples from among these are highlighted here. Botas *et al.*[132] showed that the thermal dependence of the emission peak position of luminescent silicon nanoparticles may provide primary thermometry over the 13–480 K range. Previously, Thomas *et al.*[133] observed the temperature-induced change in the emission wavelength of a CdSe (ZnS):SiO_2 thin film nanocomposite (~0.11 nm K^{-1}) over the 295–525 K range. In both cases, the Varshni relation was used as an equation of state. The upconversion emission intensity ratio of SrF_2:Yb^{3+},Er^{3+} powder has been exploited by Balabhadra *et al.*[134] to propose a primary thermometer for which the need for temperature calibration is overcome by using the value of the thermometric parameter in the limit of zero optical pump excitation power.

V. CONCLUSIONS

The last decade has witnessed a nearly exponential growth in the number of published papers and patents in the field of luminescence thermometry. This reflects extensive work carried out by a large scientific community and indicates the importance of the field for current science and technology research and development. There are still many ways in which luminescence thermometry might be advanced in the future. The recent reporting of new temperature-read-out techniques and high-sensitivity probe constructions are proof that there is plenty of space for improvements, even in these basic methodological elements. Likewise, there are yet many unexplored applications for which luminescence thermometry may prove beneficial. However, the adaptation of the method for novel applications requires further extension of background scientific knowledge, due to the interdisciplinary nature of these applications, in most cases. The search for more sensitive readouts and probes should be followed by a detailed evaluation of other thermometric parameters, the temperature resolution in particular. But, above all, future development of the method must resolve its inherent problems and faults, as well as facilitate its widespread use among experts and professionals. Thus, issues such as the assessment of measurement reproducibility and health and environmental effects should be resolved so that the scientific and engineering community as a whole gains the confidence in the method.

ACKNOWLEDGMENTS

The research was funded by the Ministry of Education, Science and Technological Development of the Republic of Serbia and the National Recruitment Program of High-end Foreign Experts (Grant No. GDT20185200479) offered by the Chongqing University of Posts and Telecommunications (CQUPT), People's Republic of China.

DATA AVAILABILITY

The data that support the findings of this study are available from the corresponding author upon reasonable request.

REFERENCES

[1]P. Neubert, U.S. patent 2,071,471 (23 February 1937).
[2]P. Neubert, U.S. patent 2,085,508 (29 June 1937).
[3]S. W. Allison, Meas. Sci. Technol. **30**, 072001 (2019).
[4]A. L. Heyes and F. Beyrau, Meas. Sci. Technol. **31**, 020102 (2020).
[5]C. D. S. Brites, S. Balabhadra, and L. D. Carlos, Adv. Opt. Mater. **7**, 1801239 (2018).
[6]L. D. Carlos and F. Palacio, *Thermometry at the Nanoscale: Techniques and Selected Applications* (Royal Society of Chemistry, Cambridge, 2016).
[7]M. Dramićanin, *Luminescence Thermometry: Methods, Materials, and Applications* (Woodhead Publishing, Cambridge, 2018).
[8]J. J. Talghader, M. L. Mah, E. G. Yukihara, and A. C. Coleman, Microsyst. Nanoeng. **2**, 16037 (2016).
[9]H. Xing, W. Bu, S. Zhang, X. Zheng, M. Li, F. Chen, Q. He, L. Zhou, W. Peng, Y. Hua, and J. Shi, Biomaterials **33**, 1079 (2012).
[10]C. Wang, L. Cheng, and Z. Liu, Biomaterials **32**, 1110 (2011).
[11]P. A. Rojas-Gutierrez, S. Bhuckory, C. Mingoes, N. Hildebrandt, C. Dewolf, and J. A. Capobianco, ACS Appl. Nano Mater. **1**, 5345 (2018).
[12]X. T. Le and Y. S. Youn, Arch. Pharm. Res. **43**, 134 (2020).
[13]G. Machin, Meas. Sci. Technol. **29**, 022001 (2018).
[14]M. D. Dramićanin, Methods Appl. Fluoresc. **4**, 042001 (2016).
[15]A. H. Khalid and K. Kontis, Sensors **8**, 5673 (2008).
[16]S. W. Allison and G. T. Gillies, Rev. Sci. Instrum. **68**, 2615 (1997).
[17]M. D. Chambers and D. R. Clarke, Annu. Rev. Mater. Res. **39**, 325 (2009).
[18]E. J. McLaurin, L. R. Bradshaw, and D. R. Gamelin, Chem. Mater. **25**, 1283 (2013).
[19]D. Jaque and F. Vetrone, Nanoscale **4**, 4301 (2012).
[20]C. D. S. Brites, P. P. Lima, N. J. O. Silva, A. Millán, V. S. Amaral, F. Palacio, and L. D. Carlos, Nanoscale **4**, 4799 (2012).
[21]X. Wang, O. S. Wolfbeis, and R. J. Meier, Chem. Soc. Rev. **42**, 7834 (2013).
[22]L. H. Fischer, G. S. Harms, and O. S. Wolfbeis, Angew. Chem. Int. Ed. Engl. **50**, 4546 (2011).
[23]A. L. Heyes, J. Lumin. **129**, 2004 (2009).
[24]M. Aldén, A. Omrane, M. Richter, and G. Särner, Prog. Energy Comb. Sci. **37**, 422 (2011).
[25]M. McSherry, C. Fitzpatrick, and E. Lewis, Sens. Rev. **25**, 56 (2005).
[26]J. Brübach, C. Pflitsch, A. Dreizler, and B. Atakan, Prog. Energy Combust. Sci. **39**, 37 (2013).
[27]B. R. Reddy, I. Kamma, and P. Kommidi, Appl. Opt. **52**, B33 (2013).
[28]S. A. Wade, S. F. Collins, and G. W. Baxter, J. Appl. Phys. **94**, 4743 (2003).
[29]C. D. S. Brites, P. P. Lima, N. J. O. Silva, A. Millán, V. S. Amaral, F. Palacio, and L. D. Carlos, New. J. Chem. **35**, 1177 (2011).
[30]X. Wang, Q. Liu, Y. Bu, C.-S. Liu, T. Liu, and X. Yan, RSC Adv. **5**, 86219 (2015).
[31]L. S. de Menezes and C. B. de Araújo, J. Braz. Chem. Soc. **26**, 2405 (2015).
[32]H. Zhou, M. Sharma, O. Berezin, D. Zuckerman, and M. Y. Berezin, ChemPhysChem. **17**, 27 (2016).
[33]C. D. S. Brites, A. Millán, L. D. Carlos, and V. K. Pecharsky, in *Handbook on the Physics and Chemistry of Rare Earths*, edited by J.-C. G. Bünzli (Elsevier Science, B,V., Amsterdam, 2016), Vol. 49, pp. 339–427.
[34]M. Quintanilla and L. M. Liz-Marzan, Nano Today **19**, 126 (2018).
[35]C. Abram, B. Fond, and F. Beyrau, Prog. Energy Combust. Sci. **64**, 93 (2018).
[36]See https://www.bipm.org/utils/common/documents/jcgm/JCGM_100_2008_E.pdf for "BIPM Brochure: Evaluation of Measurement Data—Guide to the Expression of Uncertainty in Measurement."
[37]A. L. Plant and R. J. Hanisch, "Reproducibility and replicability in Science: A metrology perspective," National Academies of Sciences, Engineering and Medicine Committee on Reproducibility and Replicability in Science Report (2018), see https://www.nap.edu/resource/25303/Metrology%20Perspective%20on%20Reproducibility.pdf.
[38]E. Glais, V. Đorđević, J. Papan, B. Viana, and M. D. Dramićanin, RSC Adv. **8**, 18341 (2018).
[39]M. Back, E. Trave, J. Ueda, and S. Tanabe, Chem. Mater. **28**, 8347 (2016).
[40]J. Ueda, M. Back, M. G. Brik, Y. Zhuang, M. Grinberg, and S. Tanabe, Opt. Mater. **85**, 510 (2018).
[41]M. Back, J. Ueda, J. Xu, K. Asami, M. G. Brik, and S. Tanabe, Adv. Opt. Mater. **8**, 2000124 (2020).
[42]L. Li, F. Qin, Y. Zhou, Y. Zheng, J. Miao, and Z. Zhang, Sens. Actuators A **304**, 111864 (2020).
[43]J. Zhou, Q. Liu, W. Feng, Y. Sun, and F. Li, Chem. Rev. **115**, 395 (2015).
[44]L. Li, F. Qin, Y. Zheng, and Z. Zhang, Opt. Mater. Express **9**, 3260 (2019).
[45]L. Li, F. Qin, L. Li, H. Gao, and Z. Zhang, J. Mater. Chem. C **7**, 7378 (2019).
[46]A. Ćirić, J. Aleksić, T. Barudžija, Ž Antić, V. Đorđević, M. Medić, J. Periša, I. Zeković, M. Mitrić, and M. D. Dramićanin, Nanomaterials **10**, 627 (2020).
[47]B. del Rosal, A. Pérez-Delgado, M. Misiak, A. Bednarkiewicz, A. S. Vanetsev, Y. Orlovskii, D. J. Jovanović, M. D. Dramićanin, U. Rocha, K. U. Kumar, C. Jacinto, E. Navarro, E. M. Rodríguez, M. Pedroni, A. Speghini, G. A. Hirata, I. R. Martín, and D. Jaque, J. Appl. Phys. **118**, 143104 (2015).
[48]B. del Rosal, A. Pérez-Delgado, E. Carrasco, D. J. Jovanović, M. D. Dramićanin, G. Dražić, Á Juarranz de la Fuente, F. Sanz-Rodriguez, and D. Jaque, Adv. Opt. Mater. **4**, 782 (2016).
[49]J. Xiong, M. Zhao, X. Han, Z. Cao, X. Wei, Y. Chen, C. Duan, and M. Yin, Sci. Rep. **7**, 41311 (2017).
[50]A. S. Souza, L. A. O. Nunes, I. G. N. Silva, F. A. M. Oliveira, L. L. da Luz, H. F. Brito, M. C. F. C. Felinto, R. A. S. Ferreira, S. A. Júnior, L. D. Carlos, and O. L. Malta, Nanoscale **8**, 5327 (2016).
[51]A. Ćirić, I. Zeković, M. Medić, Ž. Antić, and M. D. Dramićanin, J. Lumin. **225**, 117369 (2020).
[52]N. C. Chang, J. B. Gruber, R. P. Leavitt, and C. A. Morrison, J. Chem. Phys. **76**, 3877 (1982).
[53]R. P. Leavitt, J. B. Gruber, N. C. Chang, and C. A. Morrison, J. Chem. Phys. **76**, 4775 (1982).
[54]K. Trejgis, R. Lisiecki, A. Bednarkiewicz, and L. Marciniak, J. Lumin. **224**, 117295 (2020).
[55]S. Zhou, X. Li, X. Wei, C. Duan, and M. Yin, Sens. Actuators B Chem. **231**, 641 (2016).
[56]X. Qiu, Q. Zhou, X. Zhu, Z. Wu, W. Feng, and F. Li, Nat. Commun. **11**, 4 (2020).
[57]M. Sekulić, V. Đorđević, Z. Ristić, M. Medić, and M. D. Dramićanin, Adv. Opt. Mater. **6**, 1800552 (2018).
[58]Y. Lin, L. Zhao, B. Jiang, J. Mao, F. Chi, P. Wang, C. Xie, X. Wei, Y. Chen, and M. Yin, Opt. Mater. **95**, 109199 (2019).
[59]C. Matuszewska, K. Elzbieciak-Piecka, and L. Marciniak, J. Phy. Chem. C **123**, 18646 (2019).
[60]K. Elzbieciak, A. Bednarkiewicz, and L. Marciniak, Sens. Actuators B **269**, 96 (2018).
[61]Y. Chen, J. He, X. Zhang, M. Rong, Z. Xia, J. Wang, and Z.-Q. Liu, Inorg. Chem. **59**, 1383 (2020).
[62]D. Chen, S. Liu, Y. Zhou, Z. Wan, P. Huang, and Z. Ji, J. Mater. Chem. C **4**, 9044 (2016).
[63]Y. Zhou, L. Li, F. Qin, and Z. Zhang, Opt. Express **28**, 14366 (2020).
[64]I. E. Kolesnikov, D. V. Mamonova, A. A. Kalinichev, M. A. Kurochkin, V. A. Medvedev, E. Y. Kolesnikov, E. Lähderanta, and A. A. Manshina, Nanoscale **12**, 5953 (2020).
[65]M. Li, F. You, C. Liang, and Z. He, J. Alloys Compd. **833**, 155011 (2020).
[66]D. Avram, C. Colbea, M. Florea, and C. Tiseanu, J. Alloys Compd. **785**, 250 (2019).
[67]Y. Pan, X. Xie, Q. Huang, C. Gao, Y. Wang, L. Wang, B. Yang, H. Su, L. Huang, and W. Huang, Adv. Mater. **30**, 1705256 (2018).
[68]S. Wang, S. Westcott, and W. Chen, J. Phys. Chem. B **106**, 11203 (2002).
[69]D. Parobek, B. J. Roman, Y. Dong, H. Jin, E. Lee, M. Sheldon, and D. H. Son, Nano Lett. **16**, 7376 (2016).
[70]M. G. Nikolić, Ž Antić, S. Ćulubrk, J. M. Nedeljković, and M. D. Dramićanin, Sens. Actuators B Chem. **201**, 46 (2014).
[71]M. D. Dramićanin, Ž Antić, S. Ćulubrk, S. P. Ahrenkiel, and J. Nedeljković, Nanotechnology **25**, 485501 (2014).

[72]S. Ćulubrk, V. Lojpur, S. P. Ahrenkiel, J. M. Nedeljković, and M. D. Dramićanin, J. Lumin. **170**, 395 (2016).
[73]S. Das, S. Som, C.-Y. Yang, S. Chavhan, and C.-H. Lu, Sci. Rep. **6**, 25787 (2016).
[74]V. Lojpur, M. G. Nikolić, D. Jovanović, M. Medić, Ž Antić, and M. D. Dramićanin, Appl. Phys. Lett. **103**, 141912 (2013).
[75]H. Kusama, O. J. Sovers, and T. Yoshioka, Jpn. J. Appl. Phys. **15**, 2349 (1976).
[76]U. Rocha, C. J. da Silva, W. F. Silva, I. Guedes, A. Benayas, L. M. Maestro, M. A. Elias, E. Bovero, F. C. J. M. van Veggel, J. A. G. Solé, and D. Jaque, ACS Nano **7**, 1188 (2013).
[77]H. Peng, H. Song, B. Chen, J. Wang, S. Lu, X. Kong, and J. Zhang, J. Chem. Phys. **118**, 3277 (2003).
[78]R. Liang, R. Tian, W. Shi, Z. Liu, D. Yan, M. Wei, D. G. Evans, and X. Duan, Chem. Commun. **49**, 969 (2013).
[79]S. Li, K. Zhang, J.-M. Yang, L. Lin, and H. Yang, Nano Lett. **7**, 3102 (2007).
[80]G. Särner, M. Richter, and M. Aldén, Opt. Lett. **33**, 1327 (2008).
[81]A. Ćirić, S. Stojadinović, and M. D. Dramićanin, Sens. Actuators A Phys. **295**, 450 (2019).
[82]I. E. Kolesnikov, A. A. Kalinichev, M. A. Kurochkin, E. V. Golyeva, E. Y. Kolesnikov, A. V. Kurochkin, E. Lähderanta, and M. D. Mikhailov, Sci. Rep. **7**, 18002 (2017).
[83]A. Marciniak, A. Bednarkiewicz, D. Hreniak, and W. Strek, J. Mater. Chem. C **4**, 11284 (2016).
[84]D. K. Amarasinghe and F. A. Rabuffetti, Chem. Mater. **31**(24), 10197 (2019).
[85]P. H. González, L. M. Maestro, L. I. R. Martín, J. G. Solé, and D. Jaque, Small **8**, 2652 (2012).
[86]R. M. Ranson, E. Evangelou, and C. B. Thomas, Appl. Phys. Lett. **72**, 2663 (1998).
[87]V. Lojpur, Ž. Antić, and M. D. Dramićanin, Phys. Chem. Chem. Phys. **16**, 25636 (2014).
[88]C. Lin, M. T. Berry, R. Anderson, S. Smith, and P. S. May, Chem. Mater. **21**, 3406 (2009).
[89]H.-W. Song, H.-P. Xia, B.-J. Sun, S.-Z. Lu, Z.-X. Liu, and L.-X. Yu, Chin. Phys. Lett. **23**, 474 (2006).
[90]H. Liu, M. K. G. Jayakumar, K. Huang, Z. Wang, X. Zheng, H. Ågren, and Y. Zhang, Nanoscale **9**, 1676 (2017).
[91]J. R. Lakowicz, *Principles of Fluorescence Spectroscopy*, 3rd ed. (Springer, New York, 2006).
[92]T. Senden, R. D. van Moes, and A. Meijerink, Light Sci. Appl. **7**, 8 (2018).
[93]A. M. Srivastava, H. A. Comanzo, S. Camardello, S. B. Chaney, M. Aycibin, and U. Happek, J. Lumin. **129**, 919 (2009).
[94]M. D. Dramićanin, B. Milićević, V. Đorđević, Z. Ristić, J. Zhou, D. Milivojević, J. Papan, M. G. Brik, C.-G. Ma, A. M. Srivastava, and M. Wu, ChemistrySelect **4**, 7067 (2019).
[95]R. G. Geitenbeek, H. W. de Wijn, and A. Meijerink, Phys. Rev. Appl. **10**, 064006 (2018).
[96]M. Suta, Ž Antić, V. Đorđević, S. Kuzman, M. D. Dramićanin, and A. Meijerink, Nanomaterials **10**, 543 (2020).
[97]A. Ćirić, S. Stojadinović, and M. D. Dramićanin, J. Lumin. **216**, 116749 (2019).
[98]J. C. Védrine, ChemSusChem **12**, 577 (2019).
[99]I. Yarulina, A. D. Chowdhury, F. Meirer, B. M. Weckhuysen, and J. Gascon, Nat. Catal. **1**, 398 (2018).
[100]S. Pfaff, H. Karlsson, F. A. Nada, E. Lundgren, and J. Zetterberg, J. Phys. D Appl. Phys. **52**, 324003 (2019).
[101]R. G. Geitenbeek, A.-E. Nieuwelink, T. S. Jacobs, B. B. V. Salzmann, J. Goetze, A. Meijerink, and B. M. Reactions, ACS Catal. **8**, 2397 (2018).
[102]T. Hartman, R. G. Geitenbeek, G. T. Whiting, and B. M. Weckhuysen, Nat. Catal. **2**, 986 (2019).
[103]J. F. Li, Y. F. Huang, Y. Ding, Z. L. Yang, S. B. Li, X. S. Zhou, F. R. Fan, W. Zhang, Z. Y. Zhou, D. Y. Wu, B. Ren, Z. L. Wang, and Z. Q. Tian, Nature **464**, 392 (2010).
[104]S.-Y. Ding, J. Yi, J.-F. Li, B. Ren, D.-Y. Wu, R. Panneerselvam, and Z.-Q. Tian, Nat. Rev. Mater. **1**, 16021 (2016).
[105]G. Fair, T. Parthasarathy, and R. Kerans, U.S. patent 7,080,939 B1 (15 July 2006).
[106]C. Lempereur, R. Andral, and J. Y. Prudhomme, Meas. Sci. Technol. **19**, 105501 (2008).
[107]A. Rabhiou, Ph.D. thesis, Imperial College London (2012).
[108]A. L. Heyes, A. Rabhiou, J. P. Feist, and A. Kempf, AIP Conf. Proc. **1552**(1), 891 (2013).
[109]E. B. Copin, X. Massol, S. Amiel, T. Sentenac, Y. L. Maoult, and P. Lours, Smart Mater. Struct. **26**, 015001 (2017).
[110]A. Rabhiou, A. Kempf, and A. Heyes, Sens. Actuators B Chem. **177**, 124 (2013).
[111]Á. Y. González, S. Skinner, F. Beyrau, and A. L. Heyes, Heat Transfer Eng. **36**, 1275 (2015).
[112]J. Wu, T. Y. Kwok, X. Li, W. Cao, Y. Wang, J. Huang, Y. Hong, D. Zhang, and W. Wen, Sci. Rep. **3**, 3321 (2013).
[113]R. G. Geitenbeek, J. C. Vollenbroek, H. M. H. Weijgertze, C. B. M. Tregouet, A. Nieuwelink, C. L. Kennedy, B. M. Weckhuysen, D. Lohse, A. van Blaaderen, A. van den Berg, M. Odijk, and A. Meijerink, Lab Chip **19**, 1236 (2019).
[114]N. Fuhrmann, E. Baum, J. Brübach, and A. Dreizler, Rev. Sci. Instrum. **82**, 104903 (2011).
[115]L. Yan, Y. Song, W. Liu, Z. Lv, and Y. Yan, J. Appl. Phys. **127**, 124501 (2020).
[116]T. Kissel, E. Baum, A. Dreizler, and J. Brübach, Appl. Phys. B **96**, 731 (2009).
[117]S. W. Allison, D. L. Beshears, M. R. Cates, M. B. Scudiere, D. W. Shaw, and A. D. Ellis, Meas. Sci. Technol. **31**, 044001 (2019).
[118]B. R. Anderson, S. Livers, R. Gunawidjaja, and H. Eilers, Opt. Eng. **58**, 097105 (2019).
[119]M. Runowski, P. Woźny, S. Lis, V. Lavín, and I. R. Martín, Adv. Mater. Technol. **5**, 1901091 (2020).
[120]A. R. Miandashti, L. K. Khorashad, M. E. Kordesch, A. O. Govorov, and H. H. Richardson, ACS Nano **14**, 4188 (2020).
[121]D. Zhang and Q. Liu, Biosens. Bioelectron. **75**, 273 (2016).
[122]T. Pan, W. Cao, and M. Wang, Opt. Fiber Technol. **45**, 359 (2018).
[123]Z. Zhu, Anal. Chim. Acta **1054**, 122 (2019).
[124]P. E. Araque, I. M. P. V. Sansalvador, N. L. Ruiz, M. M. E. Rodriguez, M. A. C. Rodriguez, and A. M. Olmos, IEEE Sens. J. **18**, 4351 (2018).
[125]J. F. C. B. Ramalho, S. F. H. Correia, L. Fu, L. L. F. António, C. D. S. Brites, P. S. André, R. A. S. Ferreira, and L. D. Carlos, Adv. Sci. **6**, 1900950 (2019).
[126]See www.bipm.org/en/publications/si-brochure/ for "BIPM 2019 The SI Brochure," 9th ed.
[127]B. Fellmuth, J. Fischer, G. Machin, S. Picard, P. P. M. Steur, O. Tamura, D. R. White, and H. Yoon, Philos. Trans. R. Soc. A **374**, 20150037 (2016).
[128]B. Fellmuth and J. Fischer, See http://www.bipm.org/cc/CCT/Allowed/26/CCT_12-17_rev.pdf for "Document CCT/12-17/rev" (2012).
[129]Y. Zhuo, A. M. Tehrani, A. O. Oliynyk, A. C. Duke, and J. Brgoch, Nat. Commun. **9**, 4377 (2018).
[130]M. de Jong, L. Seijo, A. Meijerink, and F. T. Rabouw, Phys. Chem. Chem. Phys. **17**, 16959 (2015).
[131]Y. P. Varshni, Physica **34**, 149 (1967).
[132]A. M. P. Botas, C. D. S. Brites, J. Wu, U. Kortshagen, R. N. Pereira, L. D. Carlos, and R. A. S. Ferreira, Part. Part. Syst. Charact. **33**, 740 (2016).
[133]D. P. Thomas, B. M. Walsh, and M. C. Gupta, Nanotechnology **22**, 185503 (2011).
[134]S. Balabhadra, M. L. Debasu, C. D. S. Brites, R. A. S. Ferreira, and L. D. Carlos, J. Phys. Chem. C **121**, 13962 (2017).